Pharmacological Research 224 (2026) 108080

Contents lists available at ScienceDirect

Pharmacological Research

journal homepage: www.elsevier.com/locate/yphrs

Low, non-psychedelic doses of psilocybin as a novel treatment for MASLD, obesity and type 2 diabetes *via* 5-HT2B receptor-dependent mechanisms

Martina Colognesi [a,1], Daniela Gabbia [a,1], Anna Signor [a], Miles Sarill [a,b], Lucia Centofanti [c], Andrea Rinaldi [b], Luciano Cascione [b], Sara Nunziata [a,d], Marco Banzato [a], Andrea Mattarei [a], Giovanna Finzi [e], Sonia Sonda [f,g], Diana Pendin [f,g], Ilaria Zanotto [a], Stefano Comai [a,g,h], Gianfranco Pasut [a], Abdullah Alajati [d], Miriam Saponaro [d], Loredana Bucciarelli [i], Maria Elena Lunati [j], Giulia Guarato [a], Ilaria Goggi [c], Stefano La Rosa [k], Camillo Morano [c], Rita Clara Paroni [c], Michele Dei Cas [c], Giuseppe Daniele [l], Marco Gentilucci [m,n], Marco Pappagallo [m,n], Andrea Alimonti [b,o,p,q,r], Paolo L. Manfredi [m], Franco Folli [c,*], Sara De Martin [a,**]

[a] *Department of Pharmaceutical and Pharmacological Sciences, University of Padua, Padua, Italy*
[b] *Institute of Oncology Research (IOR), Bellinzona, Switzerland*
[c] *Department of Health Sciences, University of Milan, Milan, Italy*
[d] *Department of Urology and Paediatric Urology, University Hospital Bonn, Bonn, Germany*
[e] *Unit of Pathology, Azienda Socio-Sanitaria Territoriale (ASST) dei Sette Laghi, Varese, Italy*
[f] *Neuroscience Institute, Italian National Research Council, Padua, Italy*
[g] *Department of Biomedical Sciences, University of Padua, Padua, Italy*
[h] *Department of Psychiatry, McGill University, Montreal, QC, Canada*
[i] *Pio Albergo Trivulzio, Milan, Italy*
[j] *Division of Endocrinology, ASST Fatebenefratelli Sacco, Milan Italy*
[k] *Unit of Pathology, Department of Medicine and Technological Innovation, University of Insubria, Varese, Italy*
[l] *Department of Clinical and Experimental Medicine, University of Pisa, Pisa, Italy*
[m] *MGGM Therapeutics, Kerhonkson, New York, USA*
[n] *Albert Einstein College of Medicine, Bronx, NY, USA*
[o] *Faculty of Biomedical Sciences, Università della Svizzera Italiana, Lugano, Switzerland*
[p] *Department of Health Sciences and Technology, ETH Zurich, Zurich, Switzerland*
[q] *Department of Medicine, University of Padova, Padova, Italy*
[r] *Oncology Institute of Southern Switzerland, Ente Ospedaliero Cantonale, Bellinzona, Switzerland*

ARTICLE INFO

Keywords:
Psilocybin
MASLD
Obesity
Type 2 Diabetes Mellitus
5-HT2

ABSTRACT

The therapeutic potential of low, non-psychedelic doses of psilocybin, a fungal tryptamine alkaloid, was investigated in metabolic disorders including obesity, type 2 diabetes mellitus (T2DM), and liver steatosis. Mice fed a high-fat/high-fructose diet received chronic treatment with psilocybin (0.05 mg/kg) for 12 weeks. Body weight, liver histology, insulin sensitivity, and skeletal muscle function were assessed, and hepatic and muscle tissues underwent transcriptomic and lipidomic analyses. The role of three serotonin receptors (5-HT2A, 5-HT2B, and 5-HT2C) in psilocybin-induced metabolic effects was examined in human cell lines using pharmacological and CRISPR/Cas9-based genetic approaches. Low-dose psilocybin reduced body-weight gain, liver steatosis, hyperglycaemia, and insulin resistance without eliciting central nervous system effects. Multi-omics analyses revealed near-complete normalization of disrupted hepatic lipid and carbohydrate metabolism pathways. Psilocybin also improved muscle strength and function, potentially through restoration of leptin sensitivity. Mechanistic studies demonstrated that these metabolic benefits were independent of the canonical psychedelic target 5-HT2A and instead resulted from antagonism of the serotonin 5-HT2B receptor in the liver. Overall,

* Correspondance to: Endocrinology and Metabolism, Department of Health Sciences, University of Milan, Milan, Italy
** Correspondence to: Department of Pharmaceutical and Pharmacological Sciences, University of Padova, Largo Meneghetti 2, Padova 35131, Italy.
E-mail addresses: franco.folli@unimi.it (F. Folli), sara.demartin@unipd.it (S. De Martin).
[1] these authors share the first co-authorship

https://doi.org/10.1016/j.phrs.2025.108080
Received 30 October 2025; Received in revised form 23 December 2025; Accepted 26 December 2025
Available online 29 December 2025

chronic low-dose psilocybin exerts broad metabolic benefits via a hepatic 5-HT2B-dependent mechanism, distinct from its psychedelic effects, supporting its potential as a novel therapeutic strategy for liver steatosis, obesity, T2DM, and sarcopenia.

1. Introduction

Psilocybin (4-phosphoryloxy-*N*,*N*-dimethyltryptamine (4-PO-DMT)) is a tryptamine alkaloid, present in fungi of the *Psilocybe* genus, known for its psychedelic effects. Psychedelic substances including psilocybin have gained renewed interest in recent years and are presently being tested in clinical trials for treatment of several psychiatric diseases like depression, post-traumatic stress disorder, addiction and anorexia nervosa. Based on published clinical studies [1–3], the psychedelic experience elicited by psychedelic psilocybin doses (approximately 15–30 mg), is considered pivotal to its potential therapeutic efficacy for psychiatric disorders, with a minority of studies investigating sub-perceptual doses (0.5–2 mg) (see NCT06560658, NCT05259943, NCT04754061, NCT05832255 at clinicaltrials.gov), although this paradigm has been recently questioned [4]. Psilocybin is generally used in the form of psilocybin-containing dry mushrooms, both at psychedelic doses by recreational users and as part of traditional medicine, and at non-psychedelic doses, for alleged psychological and health benefits, in a practice known as psilocybin microdosing [5–9]. In experimental models, central nervous system (CNS) structural changes induced by psychedelics have been ascribed to stimulation of neuronal receptor tyrosine kinase-2 (TrkB) and serotonergic pathways, possibly explaining its effectiveness for psychiatric disorders [10,11].

Psilocybin is a prodrug, and the active compound psilocin (4-hydroxy-*N*,*N*-dimethyltryptamine (4-OH-DMT)) is rapidly released by phosphatase-induced dephosphorylation in the gastrointestinal tract and then absorbed in the circulation. Psilocin is a serotonin analogue known to exert its psychedelic effects by activating the 5-HT2A serotonin receptor isoform in the CNS [12]. The serotonin receptor subtypes 2 (5-HT2) comprise two other isoforms, namely 5-HT2B and 5-HT2C. The three 5-HT2 receptor isoforms are Gαq-coupled receptors and display distinct pharmacological properties [13]. Owing to the structural similarity of psilocin to the endogenous ligand serotonin, psilocin has been shown to have high affinity also for 5-HT2B and 5-HT2C [14]. Although the three 5-HT2 receptor isoforms are widely expressed inside and outside the CNS [15], the full spectrum of psilocin activity at each specific 5-HT2 isoforms in its CNS or extra-CNS effects has not been fully elucidated. In this context, research investigating psilocybin activity outside of the CNS, including its potential effects on body weight and feeding behavior, is limited and has produced mixed results [16–18]. Furthermore, because of its high affinity for the isoform 5-HT2B, researchers have cautioned that chronic psilocybin use may be a risk factor for the development of valvular heart disease, similarly to the 5-HT2B agonists pergolide and cabergoline [19].

According to recent data, when not associated to alcohol abuse, steatotic liver disease affects around 30 % of the global population and is mainly driven by obesity and type 2 diabetes mellitus [20], as indicated by its recent denomination metabolic-associated steatotic liver disease (MASLD) [21]. Considerable efforts are underway to understand the pathogenesis of metabolic disorders, with the final aim of expanding the treatment modalities for these pandemics [22]. In this context, the serotonergic system, due to its pivotal role in the physiological control of energy expenditure and metabolism, has emerged as a fascinating pharmacological target. In mammals, serotonin exerts a double effect, acting in both the CNS, by suppressing appetite [23], and in the periphery, by enhancing the absorption and storage of nutrients [24]. Thus, since peripheral serotonin acts as an endocrine factor able regulate energy storage [25,26], serotonin signaling represents a potential drug target for obesity, MASLD, and type 2 diabetes [27,28].

In patients with metabolic disorders, the loss of skeletal muscle mass and function defined as dysmetabolic sarcopenia, can be present and worsened by drugs, for examples those currently used for the treatment of obesity [29]. Sarcopenia is associated with insulin resistance and glucose intolerance [30]. The mechanisms of muscle loss in metabolic disorders have been only partially understood and are partly related to an unbalanced regulation of muscle protein turnover. An imbalance between synthesis and degradation of muscle proteins and their bioproducts in muscle tissue leads to muscle breakdown, and finally to sarcopenia. Plasma concentration of leptin, a hormone secreted by adipose tissue in proportion to fat mass, was found to be related to the risk of developing sarcopenia in obese patients [31]. Moreover leptin, being strongly associated to low-grade chronic inflammation, also named “meta-inflammation” [32], and to the development of metabolic syndrome, plays a fundamental role in regulating muscle mass and function and may be a viable pharmacological target for the therapy of metabolic diseases [33].

In this study we evaluated the body weight-reducing, glucose-lowering and anti-steatotic effects of chronic administration of low non-psychedelic doses of psilocybin in mice with metabolic dysfunctions induced by a high fat/high fructose diet (HFHFD) for 17 weeks. We then investigated the molecular mechanisms underlying the therapeutic effects of psilocybin using bulk transcriptomics and untargeted lipidomic analysis, and *in vitro* assays in hepatic cell lines overexpressing different serotonin receptor isoforms or engineered using the Crispr/Cas9 technique.

2. Materials and methods

2.1. In vitro studies

2.1.1. FLIPR assay

The FLIPR (Fluorometric Imaging Plate Reader) Penta assay, an intracellular calcium mobilization assay, was performed to characterize the agonist or antagonist activity of psilocin at human 5-HT2A, 5-HT2B and 5-HT2C receptors expressed in CHO-K1 (Chinese Hamster Ovary) cells in 384-well format. The recombinant 5-HT2A, 5-HT2B and 5-HT2C CHO-K1 cell lines, pharmacologically validated with reference compounds, were cultured in a humidified incubator with 5 % CO_2 in F12K medium supplemented with 10 % dialyzed, heat-inactivated fetal bovine serum, and 450 µg/mL of Geneticin (G418). The cells were grown in T175 flasks and passaged when 80–90 % of confluence was reached.

To assess the agonist activity, psilocin was tested for its ability to induce a calcium response at 5-HT2A, 2B or 2 C receptors using Cal-520 as no-washing calcium dye. The ability to inhibit the calcium response induced by a submaximal concentration (EC80) of the endogenous ligand serotonin was also evaluated by following a dual-addition FLIPR protocol (antagonism modality). The antagonist effect was not evaluated when the compound tested showed an agonist profile. The response was measured in real time upon receptor stimulation. Psilocin was profiled in 11-point titration curves in duplicate in two independent experiments including 5-HT as reference compound in each test, following a standardized protocol. Briefly, after seeding and medium removal, 5-HT2A and 5-HT2B-CHO cells were loaded for 30 min and 5-HT2C-CHO cells for 1 h at 37°C with 30 µL/well of a loading solution 1X (assay buffer containing 5 µM Cal-520 AM), 2.5 mM probenecid and 0.01 % Pluronic F-127). The loaded cell plates were transferred to the FLIPR instrument and calcium response was monitored during the two on-line addition protocols.

2.1.1.1. Cell cultures. Human hepatoblastoma-derived HepG2 cell line

and hepatocellular carcinoma HUH-7 cell line were purchased from the Leibniz Institute DSMZ. Mouse GFP-expressing embryonic fibroblast cells 3T3-L1-GFP were kindly gifted by Dr. Abdullah Alajati (University Medical Center Bonn, Bonn, Germany). Murine C2C12 skeletal myoblasts were purchased from the AddexBio Technologies. All the cell lines were used at low passage number (not exceeding 20). HepG2 and 3T3-L1-GFP cells were grown in Dulbecco's modified Eagle's medium (DMEM) (Corning, USA), HUH-7 cells were cultured in RPMI 1640 (RPMI) medium, both additioned with 10 % fetal bovine serum (FBS), 1 % L-glutamine and 1 % penicillin/streptomycin. C2C12 cells were grown in DMEM medium containing 3 % FBS, 1 % L-glutamine and 1 % penicillin–streptomycin. Cell lines were maintained at 37 °C and 5 % CO2 in a humidified incubator.

2.1.2. Effect of psilocin in in vitro models of hepatic lipid accumulation

HepG2 cells were employed as an *in vitro* model of MASLD [34]. The cells were seeded in 24-well plates on sterilized glass coverslips at a density of 3×10^4 cells/well. After adhesion, to induce lipid accumulation cells were treated with a mixture of palmitic and oleic acids (PA:OA mix, ratio 1:2, 0.1 mM, positive control) in complete medium, or with PA:OA mix added of increasing concentrations of psilocin (0.5, 5 and 10 μM) or the 5-HT2B antagonist RS-127445 (Merck KGaA, Darmstadt, Germany). Cell treated only with complete medium were used as negative control. After 24-h treatment, cells were washed with phosphate-buffered saline (PBS) and fixed with 4 % paraformaldehyde (PFA) for 20 min. After washing, HepG2 cells were permeabilized with a 0.1 % Triton X-100 for 10 min and incubated with Bodipy 493/503 (Lumiprobe, Hannover, Germany) for 1 h. Cells were then treated with ribonuclease A (2 mg/mL) for 5 min for the RNA degradation, and cell nuclei were stained with Hoechst 33342 (1 μg/mL). Coverslips were mounted using Mowiol 4–88. Cell fluorescence was analyzed by means of the ZEISS confocal microscope. The quantification of Bodipy-positive areas normalized per single cell was performed using the ImageJ software [35].

HUH-7 cells were employed as a second *in vitro* model of MASLD [36]. Cells were seeded in 24-well plates on sterilized glass coverslips at a density of 3×10^4 cells/well. After adhesion, lipid accumulation was induced with PA:OA mix (ratio 1:2, 0.25 mM, positive control) in complete medium, in presence or absence of 10 μM psilocin or the 5-HT2B antagonist RS-127445.

HepG2 cells were selected for further experiments.

2.1.3. Generation of HepG2 cells with mutant 5-HT2A

For the 5-HT2A gene editing, HepG2 cells were transfected with the PX458-KO plasmid [37] (see Supplementary Materials for details, Fig. S1) engineered to modify the expression of the 5-HT2A gene with 3 different oligonucleotide insertions (KO1, KO2, KO3; Table S1, Figs. S2 and S3), using the Lipofectamine™ 3000 Transfection Reagent (Thermo Fisher Scientific). Cells were seeded in 24-well plates at the density of 100,000 cells/well. After 72 h, the transfection was performed according to the manufacturer's protocol [38]. The plasmid-lipofectamine complex was added to the cells and incubated for 6 h at 37°C, followed by a medium change. Efficiency was evaluated at 24- and 48-hours post-transfection using fluorescence microscopy (Nikon Eclipse Ti-S) to detect the GFP-related fluorescence. Then, transfected HepG2 cells were harvested and sorted using a FACS Aria™ III Cell Sorter (BD Biosciences, Franklin Lakes, NJ, USA). GFP-positive cells were sorted into 96-well plates at a density of 4000 cells/well and cultured in DMEM supplemented with 20 % FBS, 2 % penicillin/streptomycin, and 1 % glutamine. The medium was changed to standard DMEM the following day. The PX458 plasmid without inserts was used as a control. After Sanger sequencing (see SM), we selected the KO1 clone, since the inserted mutations led to a dramatic change in the 5-HT2A structure. These cells were treated with PA:OA mix and stained with the lipophilic dye Bodipy 630/650 (Lumiprobe, Hannover, Germany) to assess the number and features of intracellular lipid droplets either in the presence or absence of psilocin.

2.1.3.1. Effect of psilocin in a 3D in vitro model of GFP expressing 3T3-L1-derived adipocytes.

To obtain 3D spheroids, 3T3-L1-GFP cells were seeded in 96-well plates round bottom ULA plates (BIOFLOAT™) at a density of 4×10^3 cells/well and centrifuged at 300 RPM for 15 min. After two days from spheroid formation, adipogenic differentiation was performed by adding 0.5 μM 3-isobutyl-1-methylxanthine (IBMX) and 0.25 μM Dexamethasone (DEXA) for the initial two days, and 1 μg/mL Insulin for 7 days (all reagents from Sigma-Aldrich, St. Louis, MO, USA. Medium was renewed every two days [39]. Adipocyte-like spheroids were either treated with vehicle or with 10 μM psilocin for 24 h. 3T3-L1-GFP preadipocytes were used as negative control. Spheroids were washed with phosphate-buffered saline (PBS) and fixed with 4 % paraformaldehyde (PFA) for 20 min. After washing, spheroids were permeabilized with a 0.3 % Triton X-100 for 15 min and incubated with 1 μg/mL Nile Red (NR) (Sigma-Aldrich, St. Louis, MO, USA) for 10 min. They were then treated with ribonuclease A (2 mg/mL) for 15 min for the RNA degradation, and cell nuclei were stained with Hoechst 33342 (1 μg/mL). Cell fluorescence was immediately analyzed by means of the ZEISS confocal microscope. The quantification of NR-positive areas normalized per single cell was performed using the ImageJ software [35].

2.1.3.2. Effect of psilocin in an in vitro model of myosteatosis.

C2C12 cells were seeded in 24-well plates on sterilized glass coverslips at a density of 5×10^4 cells/well. After reaching confluence, C2C12 myoblasts were differentiated into myotubes by replacement of complete medium with DMEM medium containing 2 % horse serum (HS) (Corning, USA), 1 % L-glutamine and 1 % penicillin/streptomycin. Medium was maintained for 8 days and refreshed every two days [40]. To induce myosteatosis, cells were treated with 50 μM PA and 100 μM OA (positive control) in 2 % HS complete medium, in presence or absence of 10 μM psilocin. After 24-h treatment, cells were washed with phosphate-buffered saline (PBS) and fixed with 4 % paraformaldehyde (PFA) for 20 min. After washing, myotubes were incubated with Bodipy650 (Lumiprobe, Hannover, Germany) for 1 h. Cells were then treated with ribonuclease A (2 mg/mL) for 10 min for the RNA degradation, and cell nuclei were stained with Hoechst 33342 (1 μg/mL). Coverslips were mounted using Mowiol 4–88. Cell fluorescence was analyzed by means of the ZEISS confocal microscope. The quantification of Bodipy-positive areas normalized per single cell was performed using the ImageJ software [35].

2.2. In vivo studies

2.2.1. Induction of metabolic dysfunctions with a high-fat high-fructose diet in C57BL/6J mice

In this study, we used c57BL6 mice since they are one of the most frequently used sex and strain for performing metabolic disease research, due to several practical and biological considerations. First, male rodents avoid the cyclic hormonal fluctuations of estrous seen in females, which can introduce or increase variability in the obtained data, and require larger sample sizes to achieve statistical power, thereby increasing the difficulty of following the 3 R principle [41]. Biologically, male mice often display more pronounced phenotypes, such as greater susceptibility to high-fat diet-induced obesity, insulin resistance, and glucose intolerance, making it easier to detect metabolic dysregulation and the effect of candidate drugs useful for these pandemics [42,43]. This animal study was approved by the Ethics Committee of the University of Padova for the welfare of laboratory animals (OPBA) and the Italian Ministry of Health (authorization n. 875/2023-PR– PR of 10/10/2023). All procedures involving animals were performed according to the institutional guidelines, complying with European Union Directive 2010/63/UE for experimental design

and analysis in pharmacology care, the ARRIVE (Animal Research: Reporting of In Vivo Experiments) guidelines, and the 3 R principle. Metabolic dysfunction was induced by feeding C57BL/6 J male mice a diet rich in fat (60 % kcal from fat), enriched with 30 % fructose in the drinking water (high-fat/high-fructose diet, HFHFD) [44,45], for 17 weeks. Animals were housed in IVC cages at controlled temperature (21–22°C) with 12-h alternating light and dark cycle and had access to food and water *ad libitum*. After the first 5 weeks of HFHFD, mice were divided into two groups, one treated with 0.05 mg/kg body weight (BW) psilocybin by oral gavage (5 days out of 7/week), and the other with vehicle (water) for the following 12 weeks. A group of C57BL/6 J male mice (n = 10) fed with standard diet and treated with vehicle was used as the healthy control group. Body weight, food and water intake were measured weekly. At sacrifice, animals were perfused with saline solution to remove blood completely, and the liver, pancreas and quadriceps were collected. Tissues were either snap-frozen and stored at −80 °C or fixed with 10 % formalin solution until further analysis.

2.2.2. Behavioral tests

A panel of behavioral tests was set up to assess the effect of both HFHFD and psilocybin microdoses on anxiety-like behavior, cognitive or memory impairments, and muscular strengths. Briefly, the *Light-Dark Box test (LDBT)* was used to assess anxiety behaviors. Mice were placed inside the light compartment of a LDB chamber, allowed to move freely between the two areas shown and time spent in the two compartments was measured.

The *T-maze test* was performed to assess the eventual effects of the diet or the treatment on the working memory. After a 5-minute training inside the T-maze, performed the day before the test, mice were placed at the cross section and left free to decide to explore the right or the left arm of the T-maze (8 repetitions).

The *Grid test* was performed to evaluate muscle strength and coordination. The mouse was placed in the center of a square metal grid, which was turned upside down. The hanging time on the grid was recorded. After fall, the mouse was returned to the center of the grid, and the session was repeated till the first sign of weakness or distress, and no longer than 10 min. Physical impulse was expressed as grams of body weight * seconds spent hanging on the grid.

2.2.3. Intraperitoneal glucose tolerance test and fasting glucose

Before sacrifice, Intraperitoneal Glucose Tolerance test (IpGTT) was performed after a six-hours fasting in mice challenged with i.p. glucose (1 g/Kg BW). Blood glucose was measured using a glucometer at baseline and 15, 30, 60, 90 and 120 min after administration. Insulin plasma levels were measured by a Rat/Mouse Insulin ELISA kit (EZRMI-13K, Millipore, Burlington, MA, USA).

2.2.4. Circulating hormones and incretins and glycogen

The plasma concentrations of c-peptide, glucagon, pancreatic polypeptide, amylin, glucagon-like Peptide 1 (GLP-1), glucose-dependent insulinotropic polypeptide (GIP), polypeptide YY, leptin and resistin were measured by the MILLIPLEX® *Mouse Metabolic Hormone Expanded Panel* (EMD Millipore, Billerica, MA, USA, Cat. # MMHE-44K) on samples collected at sacrifice. Hepatic glycogen was quantified by means of glycogen assay kit (MAK465, Sigma-Aldrich, St. Louis, MO, USA).

2.2.5. Histological analysis of liver tissue

Liver tissues were paraffin-embedded to perform histological analysis by the hematoxylin and eosin (H&E) staining using 5 μm thick sections. To analyze insulin receptor substrate 1 (Irs-1) protein expression, immunohistochemical analyses were performed on 5-μm hepatic tissue sections by using an anti-Irs-1 antibody (Table S2). DAB was used as a substrate [46]. A portion of frozen liver tissue was included in Optimal Cutting Temperature (OCT) and cryosections of 10 μm were stained with Oil Red O (ORO) staining [47]. Images were captured using a Nikon Eclipse Ti-S microscope (Nikon Europe, Amstelveen, The Netherlands) and analyzed with the ImageJ software. Triglycerides hepatic content was measured by means of the Triglycerides CP ABX Pentra HORIBA kit and quantified using VICTOR Nivo Multimode Microplate Reader spectrophotometer (absorbance 520 nm).

2.2.6. Transmission electron microscopy (TEM)

At sacrifice, pancreas tissues of two healthy controls, two HFHFD and two psilocin-treated HFHFD mice were fixed in a mixture of 2 % PFA and 2,5 % glutaraldehyde in 0.005 M sodium cacodylate buffer (pH 7.4) then post-fixed in 1 % OsO_4 in 0.1 M sodium cacodylate buffer (pH 7.4), and, after dehydration in graded series of ethanol, were transferred to propylene oxide and embedded in Epon-NMA resin [48]. Section of 100 nm thick were cut and mounted on nickel grids and stained with uranyl acetate and lead citrate. For ultrastructural immunocytochemistry, pancreas tissues were fixed in a mixture of 2 % paraformaldeyde and 0, 5 % glutaraldehyde in 0.005 M sodium cacodylate buffer (pH 7.4) and embedded in London White Resin. Sections were put onto a drop of 1 % ovoalbumine, then transferred onto a drop of Dako polyclonal guinea pig anti-insulin antibody diluted 1:50 overnight, after rinses in 0.05 M TBS buffer pH 7.4 were put onto a drop of 12 nm colloidal gold AffiniPureDonkey anti-guinea pig (Jackson Immuno Research) diluted 1:50, and, after rinses, stained with uranyl acetate and lead citrate. Sections were examined with a JEOL 1400 Plus Transmission electron microscope [49]. The ratio of mature versus total secretory granules were evaluated by counting the granules in a selected area of a picture of each mouse studied.

2.2.7. Western blot analysis

Total proteins were extracted from liver tissues using RIPA lysis buffer supplemented with Complete Mini Protease Inhibitor Cocktail (Roche). Western blot on liver tissue lysates was performed to measure the protein expression of Akt serine/threonine kinase 1 (Akt1), its active phosphorylated form (pAkt1) and leptin receptor. A Biorad miniprotein apparatus with precast gels loaded with 30 μg of proteins per lane was used. The primary and secondary antibodies used are reported in Tab S2. Luminata was used as horseradish peroxidase (HRP) substrate (Millipore, Burlington, NA, USA). The signal intensity of immunoreactive bands was visualized by means of Azure imaging system and normalized to that of Glyceraldehyde-3-phosphate dehydrogenase (Gapdh).

2.2.8. Bulk transcriptomic analysis of liver and quadriceps

The Total RNA Purification Kit (Norgen Biotek Corp.) was used for the RNA extraction from liver samples, while the *SV Total RNA Isolation System* (Promega Corporation) was used for quadriceps. The extraction was performed according to the manufacturer's instructions, and the concentration and purity of RNA were assessed by a Nanodrop spectrophotometer.

NEBNext Ultra Directional RNA Library Prep Kit for Illumina (New England BioLabs Inc.) was employed with the NEBNext Multiplex Oligos for Illumina (New England BioLabs Inc.) and NEBNext® Poly(A) mRNA Magnetic Isolation Module for cDNA synthesis with the addition of barcode sequences. The pre-pool sequencing was performed using the NextSeq2000 (Illumina, San Diego, CA, USA) with the P2 reagents kit V3 (100cycles; Illumina). Samples were processed starting from stranded, single-ended 120bp-long sequencing reads.

2.2.8.1. Transcriptomic data analysis. For transcriptomic data analyses, we evaluated the quality of RNA-seq reads using FastQC (v0.11.5, available online at http://www.bioinformatics.babraham.ac.uk/projects/fastqc) and removed low-quality reads/bases and adaptor sequences using Trimmomatic (v0.35) [50]. The resulting high-quality trimmed reads were aligned to the mouse reference genome (mm10) using STAR [51], a spliced-read aligner that supports the alignment of reads spanning multiple exons. Samples were considered of good quality if more than 85 % of sequencing reads aligned to the reference genome. Gene

expression quantification was performed using HTSeq-count [52] with NCBI gene annotation for mm10 as reference. Expression values were provided in tab-delimited format. We filtered the dataset to retain genes with counts-per-million (CPM) values greater than 5 in at least half of the samples. The data were normalized using the TMM (trimmed mean of M-values) method from the edgeR package [53] and transformed to log2 CPM using the cpm function. Differential gene expression for each comparison of interest was computed using limma, following TMM normalization and voom transformation [54]. To investigate pathway-level changes, we performed gene set enrichment analysis (GSEA) [55] and gene set variation analysis (GSVA) [56] using the clusterProfiler R package [57]. For both analyses, we utilized gene sets from the Molecular Signatures Database (MSigDB) [58]. These complementary approaches allowed us to assess both enrichment of predefined gene sets and sample-wise variation in pathway activity. STRING networks were produced with the stringApp (version 2.2.0) in Cytoscape (version 3.10.3). The STRING network for GOBP Lipid Localization was filtered for liver expression, decreasing the number of nodes displayed [59]. Normalized enrichment scores and FDR q-values were calculated using GSEA preranked (GSEA version 4.3.3). The data were visualized as Lollipop plots using RStudio (version RStudio 2024.12.1 +563) with ggplot2 and clusterProfiler packages [60]. Volcano plots of differentially expressed genes from the quadriceps and liver transcriptomic data were created using MaGIC Volcano Plot Tool (https://volcano.bioinformagic.tools/).

2.2.9. Lipidomic analysis of liver tissue

2.2.9.1. Chemicals and reagents. The chemicals acetonitrile, 2-propanol MS-grade, acetonitrile MS-grade, methanol, chloroform, formic acid MS-grade, ammonium acetate MS-grade were purchased from Sigma-Aldrich (St. Louis, MO, USA). All aqueous solutions were prepared using purified water at a Milli-Q grade (Burlington, MA, USA).

2.2.9.2. Extraction from liver tissue samples. An aliquot of liver tissue (approximately 100 mg) was diluted with 100 μL of water and homogenized by Tissue Lyser at 50 Hz for 3 rounds of 5 min with 5 min of rest in ice. Protein content was assessed by the BCA protein assay kit (ThermoFisher), and the amount of tissue homogenate equivalent to 500 ug was diluted to 100 μL with the addition of H_2O. Total lipid content was extracted by 850 μL of a methanol/chloroform mixture (2:1, v/v) [61]. 5 μL of organic extract (IPA/AcN + 0.05 % BHT) was loaded on column for each analysis.

Addition of butylated hydroxytoluene (BHT) during sample preparation avoided unspecific oxidation [62,63].

2.2.9.3. Untargeted lipidomics. LC-MS/MS consisted of a Shimadzu LC40 XR UHPLC System coupled with a Triple TOF X500B (Concord, ON, CA) equipped with Turbo V ion source. All samples were analyzed in duplicate in both positive and negative mode with electrospray ionization (ESI). Spectra were contemporarily acquired by full-mass scan from 200 to 2000 *m/z* and top-20 data-dependent acquisition, with dynamic background subtraction, from 50 to 2000 *m/z*. The accumulation time were for TOF-MS 100 ms and for TOF MS/MS 40 ms with a total scan time of less than 1 s. Declustering potential was fixed to + /- 60 eV, and the collision energy was + /- 35 ± 15 eV. Electrospray ionization voltages were set at 5.5 and −4.5 kV. The source and gas parameters were: GS1 55 psi, GS2 65 psi, Curtain gas 35 psi and temperature 500 °C. The chromatographic separation was reached on a reverse-phase Acquity CSH C18 column 1.7 μm, 2.1 × 100 mm (Waters, Franklin, MA, USA) equipped with a precolumn by a gradient between (A) water/acetonitrile (60:40) and (B) 2-propanol/acetonitrile (90:10), both containing 10-mM ammonium acetate and 0.1 % of formic acid. The column oven temperature was 55 °C with a constant flow of 0.3 mL/min. Gradient details were the following (%B): 0 min 40 %, 2 min 40 %, 2.5 min 50 %, 12.5 min 55 %, 13 min 70 %, 19 min 99 %, 24 min 99 %, 24.2 min 40 % and maintained until 30 min for reconditioning.

2.2.9.4. LC-HR-MS data processing. The spectra deconvolution, peak alignment and sample normalization were attained using MS-DIAL (ver. 4.7). MS and MS/MS tolerance for peak profile was set to 0.01 and 0.05 Da, respectively. Identification was achieved by matching spectra with LipidBlast database or in-house built mass spectral library. Intensities of analytes were normalized by LOWLESS algorithm and those with a CV% superior to 30 % in the QC pool sample were excluded. Mass spectrometry performances during the batch were monitored by the intensities of deuterated internal standard mix (EQUISPLASH™ LIPIDOMIX™ QUANTITATIVE MASS SPEC INTERNAL STANDARD, Avanti polar, AL, USA). The commercial mixture was fortified with another deuterated lipid standards for a better lipidome coverage: C14:0 L-carnitine-d9, Oleic acid-d9, Cholesterol-d7 (Avanti polar, AL, USA).

2.2.9.5. Stepwise multivariate regression analysis. To identify specific hepatic lipid species associated with insulin resistance, a stepwise multiple linear regression analysis was conducted with HOMA-IR and with glucose as the dependent variables separately. For each experimental group (Standard Diet, HFHFD, and HFHFD + Psilocybin), the relative abundance of individual liver lipid species was used as independent predictors. Both forward and backward stepwise selection was applied using Bayesian Information Criterion (BIC) to determine the most parsimonious models. This approach enabled the isolation of the most informative lipids contributing to interindividual variation in HOMA-IR and glucose, under different metabolic conditions.

2.3. Statistical analysis

Statistical analyses were performed by GraphPad Prism software, ver. 10.4.1 (GraphPad Software Inc., San Diego, CA, USA) and with MetaboAnalyst 6.0. Experimental data have been compared by one-way or two-way ANOVA, or the Wilcoxon Mann-Whitney test, as appropriate. ANOVA was followed up by the Tukey's or the Bonferroni post-hoc tests. A value of $p < 0.05$ was considered statistically significant. Unless otherwise stated, data are expressed as means ± S.E.M.

3. Results

3.1. Low, nonpsychedelic doses of psilocybin reduce body weight increase in HFHFD mice, without detrimental central nervous system effects

The administration of 0.05 mg/kg of psilocybin for 12 weeks (Fig. 1A) significantly reduced the increase of body weight induced by the HFHF diet (Fig. 1B-C, mixed effect analysis, time: $F(1.916, 45.34) = 77.03$, $p < 0.0001$; treatment: $F(2, 24) = 19.1$, $p < 0.0001$; treatment: $F(2, 24) = 19.1$, $p < 0.0001$; interaction: $F(24, 284) = 9.682$, $p < 0.0001$). This reduction was achieved without significant changes in food and water intake, although a decreasing trend could be observed in psilocybin-treated mice (Fig. 1D). The light-dark box test showed that time before entering the dark chamber was increased by psilocybin treatment, suggesting a potential anti-anxiety effect (Fig. 1G). No significant effect was observed on the percentage of correct alternation in the T-maze test, although the median value in healthy controls and psilocybin treated mice was higher than that of HFHFD mice (86 % for healthy controls and psilocybin-treated, vs 71 % for HFHFD-fed mice).

3.2. Low, nonpsychedelic doses of psilocybin reduce MASLD by normalizing hepatic lipid storage and composition and ameliorate insulin sensitivity

Liver histology and steatosis were markedly improved by psilocybin, as demonstrated by the H&E (Fig. 2A) and the ORO (Fig. 2B) staining.

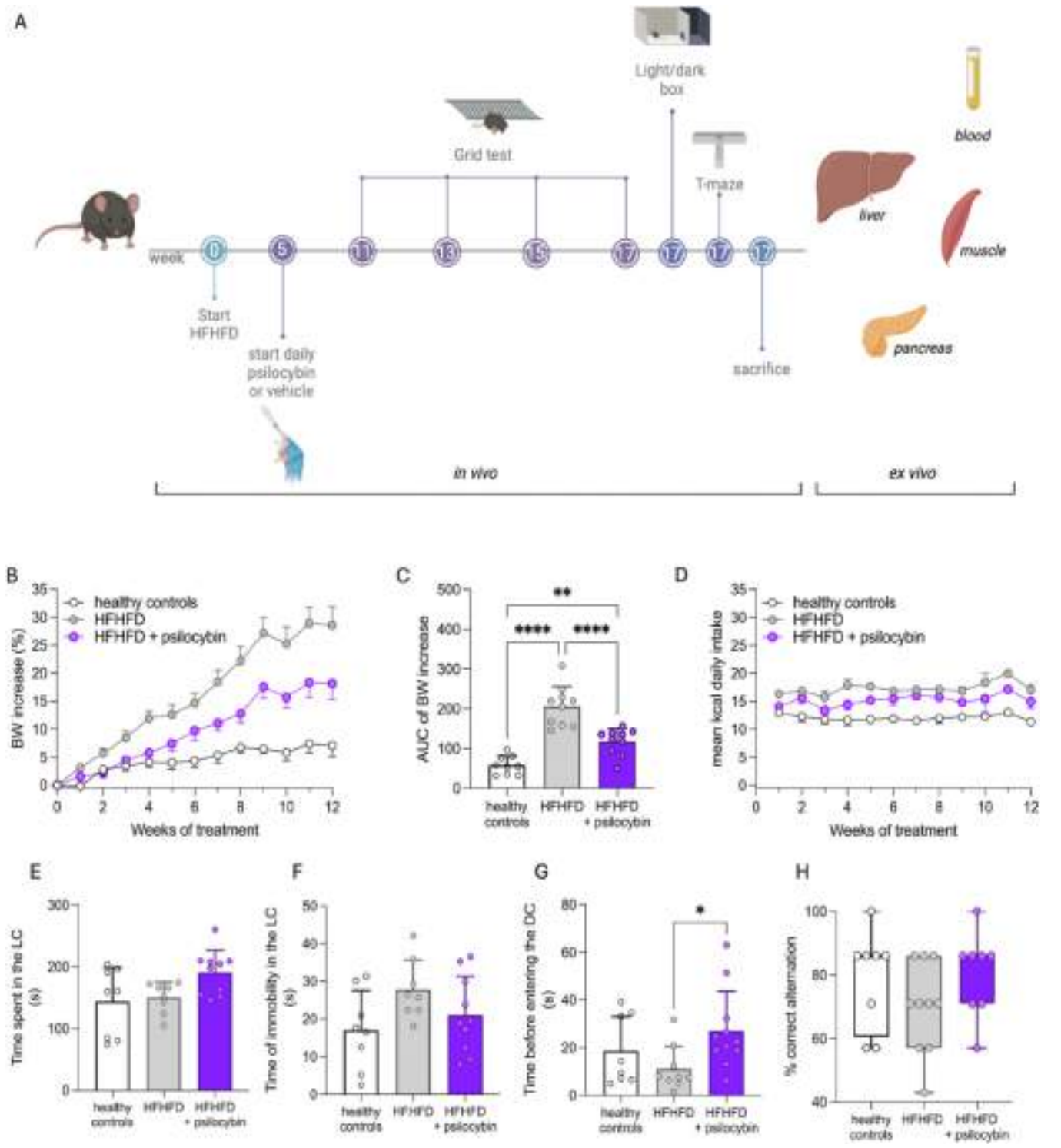

Fig. 1. Psilocybin effect on body weight increase and behavioral and muscular performance in HFHFD-fed mice. A Schematic representation of the experimental workflow, including pharmacological treatment schedule and behavioral tests (Created in Biorender, https://www.biorender.com/). B Evaluation of body weight (BW) increase and (C) relative area under the curves (AUCs) from the beginning of the pharmacological treatment (n = 9 [healthy controls], n = 10 [HFHFD and HFHFD + psilocybin]). **p < 0.01, and ****p < 0.0001. D Daily mean kcalories consumption per mouse, derived from fructose and food intake, from the beginning of the pharmacological treatment. E-G Assessment of anxiety-like behavior using the light-dark box test (n = 8 [healthy controls and HFHFD], n = 10 [HFHFD + psilocybin]), considering parameters e.g. (E) total time spent in the light compartment (LC), (F) immobility time in the LC and (G) latency to enter into the dark compartment (DC) the first time. *p < 0.05 H Percentage of spontaneous alternation during the T-maze test. All data are presented as mean ± S.E.M.

Lower liver weight (Fig. 2C) and triglycerides content (Fig. 2D) were also measured in psilocybin-treated mice as compared to untreated HFHFD mice. The positive impact on liver lipids exerted by psilocybin was further confirmed by the gene set variation analysis (GSVA) of the bulk transcriptomic data of liver tissue. The gene sets involved in lipid localization, storage and lipid droplet organization were all upregulated by the HFHFD and normalized in HFHFD-fed mice treated with psilocybin (Fig. 2E-H). The expression of genes involved in lipid import into

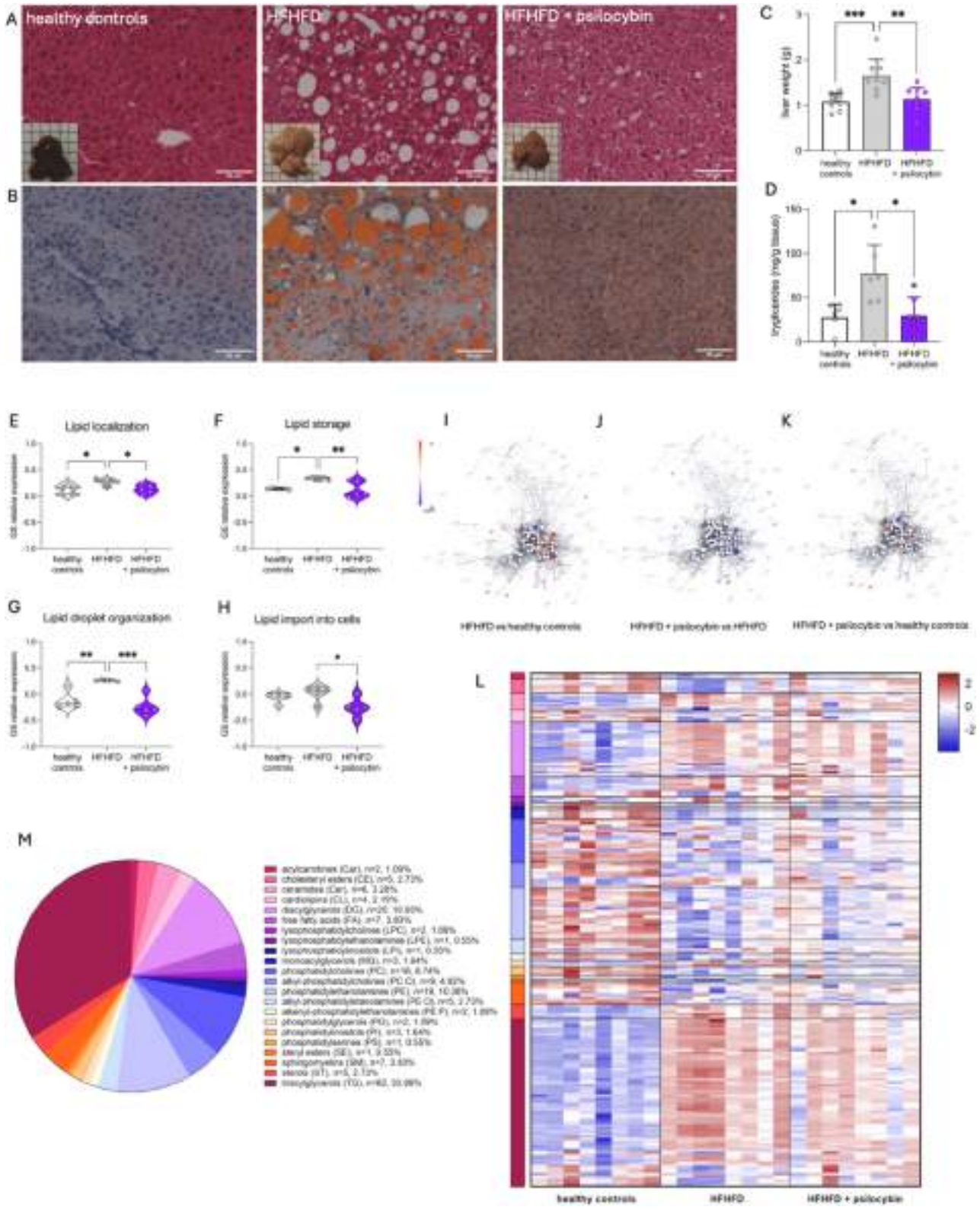

Fig. 2. Psilocybin effect on liver steatosis and hepatic biological processes involved in lipid storage, metabolism and oxidation. A-B Representative liver photos and sections after staining with (A) hematoxylin and eosin (H&E) and (B) oil red O (ORO) stain, 20x magnification. C-D Liver weight assessment (n = 8 [healthy controls], n = 9 [HFHFD and HFHFD + psilocybin]) and (D) hepatic triglycerides content (n = 6 [healthy controls and HFHFD], n = 7 [HFHFD + psilocybin]). E-H Violin plot representing the main hepatic gene sets modulated by psilocybin treatment, e.g. (E) lipid localization, (F) lipid storage, (G) lipid droplet organization, (**H**) lipid import into cells (n = 5). *p < 0.05, **p < 0.01, ***p < 0.001. I-K STRING network representing the differentially expressed genes identified from the comparison of bulk RNAseq of liver tissue of HFHFD vs healthy controls (I), HFHFD + psilocybin vs HFHFD (J), and HFHFD + psilocybin *vs* healthy controls (K). The scalebar shows color mapping representing average log_2FC. M-L Psilocybin effect on hepatic lipidome. (M) Pie and (L) heatmap chart of the 185 lipids significantly modified by psilocybin treatment after Spearman rank correlation, according to their lipid class, p value < 0.05. Numeric data are presented as mean ± S.E.M.

cells was also significantly reduced by psilocybin treatment (Fig. 2G). The STRING network for the Gene Ontology Biological Process (GOBP) Lipid Localization (Fig. 2I-J-K) showed that clusters of genes upregulated by HFHFD, such as the gene *Cidea* (Cell Death Inducing DFFA Like Effector A), were downregulated by psilocybin treatment. An untargeted lipidomic analysis revealed that 185 lipids resulted significantly ($p < 0.05$) modified by psilocybin treatment, 110 of which remained significant after false discovery rate analysis (FDR<0.05, Fig. 2L). Most lipids moieties were triglycerides (33.88 %), followed by diglycerides (10.93 %), phosphatidylethanolamines (10.38 %) and phosphatidylcholines (8.74 %) (Fig. 2L-M). Among the triglycerides, 20 (32.26 %) had at least one oxidation on their chains. Regarding the saturation of their chain, none had only saturated chains, around half (47.62 %) of the unoxidized triglycerides had one or more saturated chains, and 75 % of the oxidized triglycerides had one or more saturated chains. All the triglycerides and the fatty acids were higher in the HFHFD compared to healthy controls and were reduced by psilocybin treatment, while the others (phosphatidylcholine (PC), cholesteryl ester (CE), acylcarnitine (CAR), sterol ester (SE), and monoglyceride (MG)) were lowered by HFHFD and increased in psilocybin treated HFHFD mice (Fig. 2L). Notably, psilocybin did not influence lipid oxidation (Fig. S4A), as also observed in HepG2 cells, where psilocin, the active compound of the prodrug psilocybin, did not significantly alter any mitochondrial respiration parameter, nor did it prevent etomoxir-induced fatty acids oxidation by the mitochondrion (Fig. S4B-C).

Global transcriptomic changes in the liver were also visualized as a multidimensional scaling plot (MDS) (Fig. S5) and volcano plots (Fig. S6A). GSEA analysis of hallmark gene sets was displayed as lollipop plots (Fig. S6B) that showed that psilocybin treatment was downregulating several hallmarks which were upregulated by the HFHFD, including fatty acid metabolism, hypoxia, mechanistic target of rapamycin complex 1 (mTorc1)-signaling, and epithelial to mesenchymal transition. Hepatic glycogen was also reduced by psilocybin (Fig. 3A). Accordingly, the gene set variation analysis (GSVA) analysis demonstrated that psilocybin treatment induced a normalization of the gene set related to carbohydrate biosynthetic processes (Fig. 3E), negative regulation of glucose transmembrane transport (Fig. 3F), as well as an increase in leptin signaling response (Fig. 3G), although leptin receptor expression was unaffected by psilocybin treatment (Fig. 3C-D). Notably, total expression of Akt1 was increased in mice fed with HFHFD (Fig. 3D) and its phosphorylation showed a clear increasing tendency in psilocybin treated mice (Fig. 3B-D). Insulin receptor substrate 1 (Irs1) expression in hepatocytes was significantly downregulated in HFHFD-fed mice and normalized by psilocybin (Fig. 3H-I).

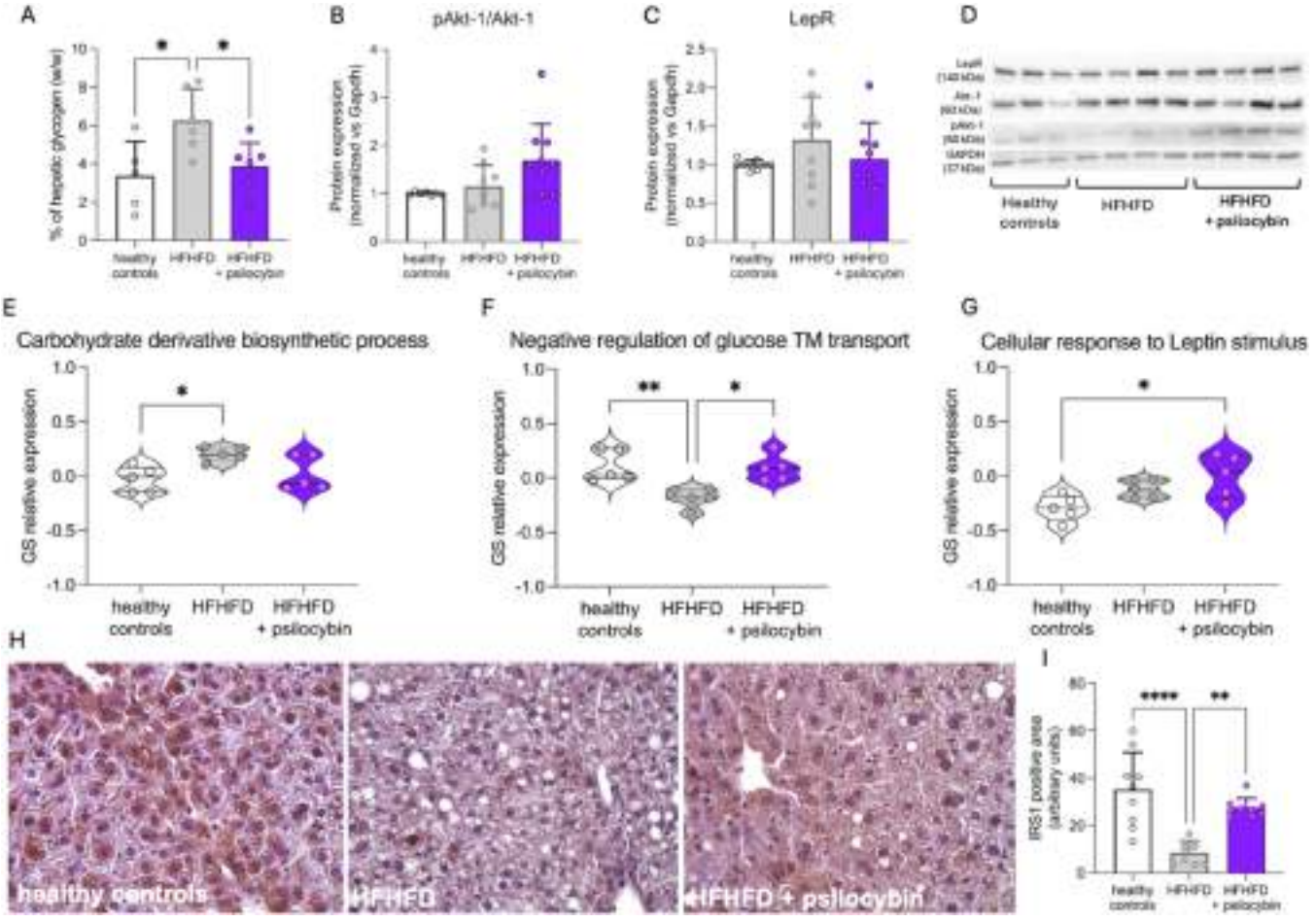

Fig. 3. Psilocybin effect on carbohydrate metabolism and leptin signaling. (A) Percentage of hepatic glycogen (w/w) (n = 5 [healthy controls], n = 6 [HFHFD], n = 7 [HFHFD + psilocybin]). *$p < 0.05$. B-D Protein expression of (B) pAkt-1/Akt1 ratio and (C) leptin receptor in liver tissue normalized vs healthy controls (n = 9 [healthy controls], n = 10 [HFHFD and HFHFD + psilocybin]), and (D) representative western blot analysis showing healthy controls, HFHFD and HFHFD + psilocybin (n = 3). *$p < 0.05$. E-G Violin plot representing hepatic mRNA transcriptome gene sets modulated by psilocybin treatment, e.g. (E) carbohydrate derivative biosynthetic process, (F) negative regulation of glucose transmembrane transport, and (G) cellular response to leptin stimulus (n = 5). *$p < 0.05$, **$p < 0.01$. H Representative images of Irs1 immunoreactivity in the liver tissue from healthy controls (n = 9), HFHFD (n = 10), and HFHF + psilocybin (n = 10) and (I) relative quantification of the 3,3′-diaminobenzidine (DAB) positive areas. **$p < 0.01$, ****$p < 0.0001$. All data are presented as mean ± S.E.M.

3.3. Low, nonpsychedelic doses of psilocybin correct hyperglycemia, insulin resistance and gut hormones dysregulation induced by HFHFD

Psilocybin-treated mice had fasting blood glucose and insulin levels comparable to those of control mice, and significantly lower than those of HFHFD-fed mice (Fig. 4B-D). Furthermore, in the ipGTT the AUC of the plasma blood glucose was significantly higher in HFHFD as compared to control ($p < 0.05$), and similar in controls and psilocybin treated mice (Fig. 4A-E). The glucose peak was significantly higher only in HFHFD mice ($p < 0.05$), but not in psilocybin-treated mice, as compared to controls (Fig. 4A). Insulin secretion in the ipGTT was significantly increased in HFHFD mice as compared to controls ($p < 0.01$), while there were no significant differences in healthy controls and the psilocybin-treated mice (Fig. 4C-F).Whole body insulin resistance as defined by HOMA-IR increased by 3 fold in HFHFD as compared to healthy controls (5.21 ± 1.89 vs. 1.68 ± 0.75; $p < 0.01$) while psilocybin treatment dramatically dampened HOMA-IR (-3.52 ± 1.13, $p < 0.05$), being only slightly higher than that of the healthy controls (2.10 ± 1.49 vs. 1.68 ± 0.75; p = ns) (Fig. 4G).

Fasting levels of pancreatic hormones which were profoundly dysregulated by HFHFD, were normalized by psilocybin (insulin, Fig. 4F; C-peptide, Fig. 4G; pancreatic polypeptide, Fig. 4I). Plasma concentration of glucagon and amylin were unaffected by the HFHFD and by psilocybin treatment (Fig. 4H-J). Interestingly, psilocybin restored normal levels of fasting GIP, Polypeptide YY, resistin, and leptin, although had no effect on GLP-1 one (Fig. 4L-M-N-O).

Electron microscopy analysis revealed that HFHFD induced severe damage of insulin-producing β cells, which displayed reticulum and

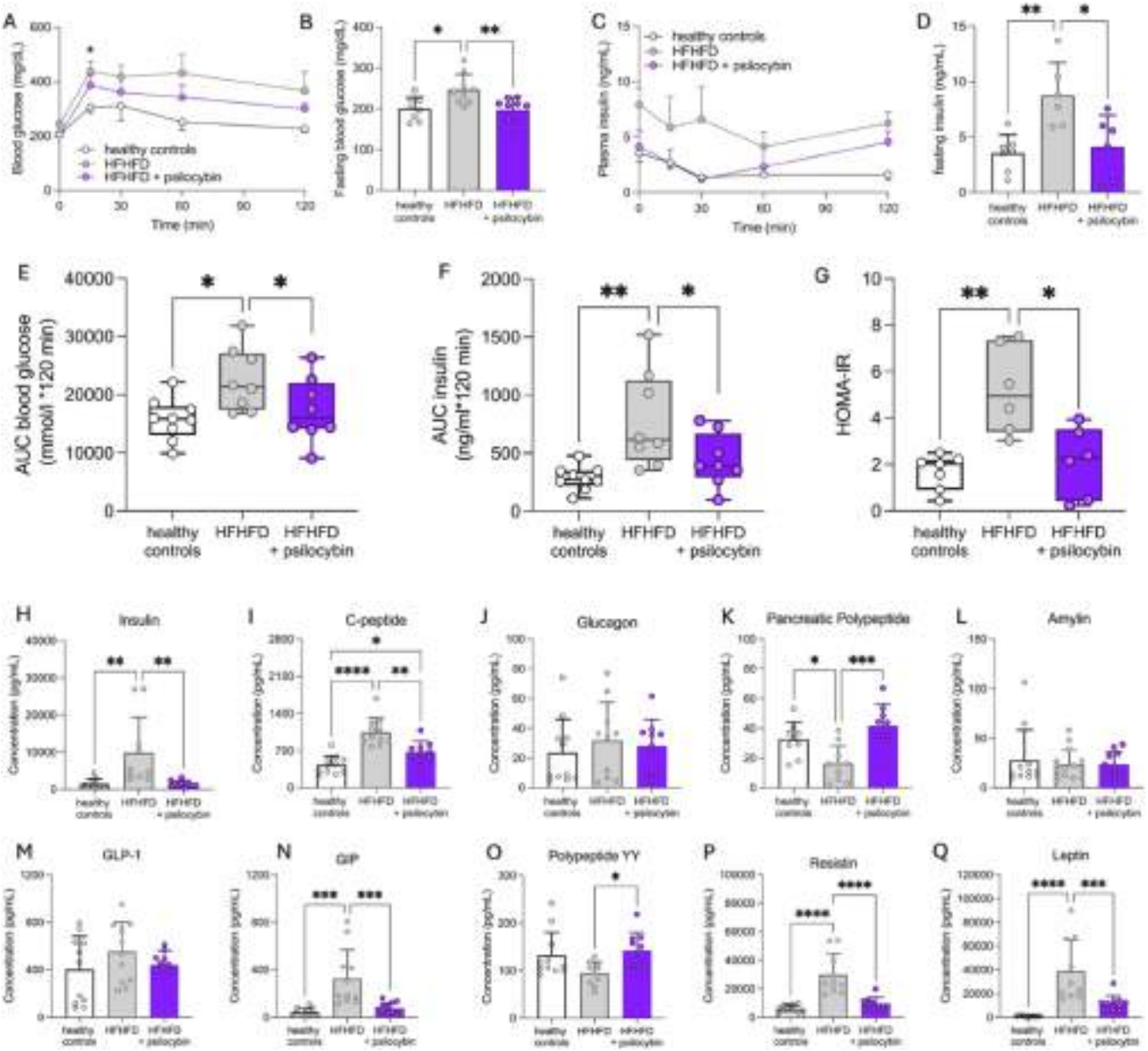

Fig. 4. Psilocybin effect on glucose uptake, insulin sensitivity and hormones involved in metabolic control. A-G Results of intraperitoneal glucose tolerance test (ipGTT) (A) during 120 min of follow-up and (B) fasting blood glucose levels. (C) Plasma insulin-vs-time curve and (D) fasting insulin; AUC of the blood glucose (E) and plasma insulin (F) vs time curves, and HOMA-IR index, calculated as HOMA-IR = [(*fasting blood glucose*, mmol/L) x (*fasting plasma insulin*, mU/L)] / 22.5 (G). H-Q Plasmatic levels of (H) insulin and other hormones involved in glycemic regulation: (I) C-peptide, (J) glucagon, (K) pancreatic polypeptide, (L) amylin, (M) GLP-1, (N) GIP, (O) polypeptide YY, (P) resistin and (Q) leptin. *$p < 0.05$, **$p < 0.01$, ***$p < 0.001$, and ****$p < 0.0001$. All data are presented as mean ± S.E.M. (n = 9 [healthy controls], n = 10 [HFHFD and HFHFD + psilocybin]).

Golgi cysternae dilatation, and markedly dilated secretory granules with lower insulin content. In contrast, the islets of Langerhans of mice fed with HFHFD and treated with psilocybin showed healthy and well granulated insulin-producing β cells (Fig. 5). The total number of insulin granules, mature granules, immature granules, and mature dilated granules were counted in two pancreases for each group (total 6 pancreas) in a photomicrograph with an area of 10 by 7,5 cm at 20000 x magnification. The total number of insulin granules was not significantly different in the three experimental groups. In both HFHFD groups there was a significant decrease in immature granules. In HFHFD animals there were no normal mature granules. Mature granules were present in similar number in healthy controls and in HFHFD-psilocybin treated mice. Furthermore, in the HFHFD pancreases, all mature granules were markedly dilated. Dilated mature granules were not present in healthy animals and in HFHFD-psilocybin. Dilatation of mature granules is a hallmark of sufferance induced by HFHFD, which is completely reversed by the treatment with psilocybin (Table S3).

3.4. The restoration of insulin sensitivity induced by low, nonpsychedelic doses of psilocybin is correlated to a remodeling of the hepatic lipidome

A peculiar lipid pattern modulation by HFHFD and psylocibin emerged from a correlation analysis using HOMA-IR and identified hepatic lipids as variable (Fig. 6). HOMA-IR correlated directly with multiple ceramides - e.g., Cer 20:0 (R^2=0.55; $p < 0.005$), DhCer 22:0 (R^2=0.58; $p < 0.003$), and Cer 18:0 (R^2=0.48; $p \approx 0.017$) - and with several diacylglycerols (e.g., DG 32:1|16:0_16:1, DG 36:2|18:1_18:1, DG 38:0|16:0_22:0; R^2=0.43–0.46; $p < 0.05$). Dozens of mid-length triglycerides (roughly C42–C54; e.g., TG [44–52] including oxidized forms) showed positive associations (typical R^2=0.40–0.55; $p < 0.05$), and sterol species were also positively related [ST 27:1;O R^2=0.47; $p < 0.021$; SE 29:1/18:2 R^2=0.43; $p < 0.040$]. Conversely, HOMA-IR was inversely associated with acylcarnitines (CAR 18:2 R^2=0.42; $p < 0.043$; CAR 20:4 R^2=; $p < 0.023$), with polyunsaturated membrane phospholipids and plasmalogens (e.g., PC O-42:5) R^2=0.46; $p < 0.004$; PC [30–36] species and PE O-36:3 R^2=0.57; $p < 0.007$; PI 34:2|16:0_18:2 R^2= 0.56; $p < 0.005$), and with very-long-chain, highly unsaturated TGs (e.g., TG 66:4|16:1_32:1_18:2, R^2=0.48; $p < 0.018$; TG 66:6|16:0_16:0_34:6, R^2=0.45; $p < 0.028$). Stepwise multivariate regression identified distinct hepatic lipid signatures predictive of HOMA-IR in each experimental group. In healthy controls, the model (R^2=1.00) was dominated by neutral storage lipids - diacylglycerol DG 32:3|14:1_18:2, triacylglycerols TG 74:2|18:0_18:1_38:1, TG 46:4|16:0_14:1_16:3, TG 66:2|16:0_18:1_32:1, and the ether phosphatidylethanolamine PE O-36:3|18:1_18:2 - together with Cer 18:0. In HFHFD mice, the predictive profile (R^2=1.00) shifted toward a more lipotoxic composition, including Cer 20:0, multiple TGs enriched in saturated and monounsaturated fatty acids (TG 48:3|14:0_16:1_18:2, TG 46:4|16:0_14:1_16:3, TG 48:3;2 O|16:0_16:0_16:3;2 O), a sterol ester (SE 28:1/18:1), and the free sterol ST 27:1;O. In HFHFD mice treated with psilocybin, the model (R^2=1.00) retained three ceramides (Cer 20:0, Cer 18:0, DhCer 22:0) but introduced highly unsaturated membrane lipids (PC 36:5|18:2_18:3, PE 42:5|22:1_20:4) and the sterol ST 27:1;O. Similar observations were evident from the correlation analysis between fasting glucose and hepatic lipids, which showed that high fasting glucose levels are associated with a coherent, lipotoxic lipid pattern, and reduced by psilocybin (Fig. S7).

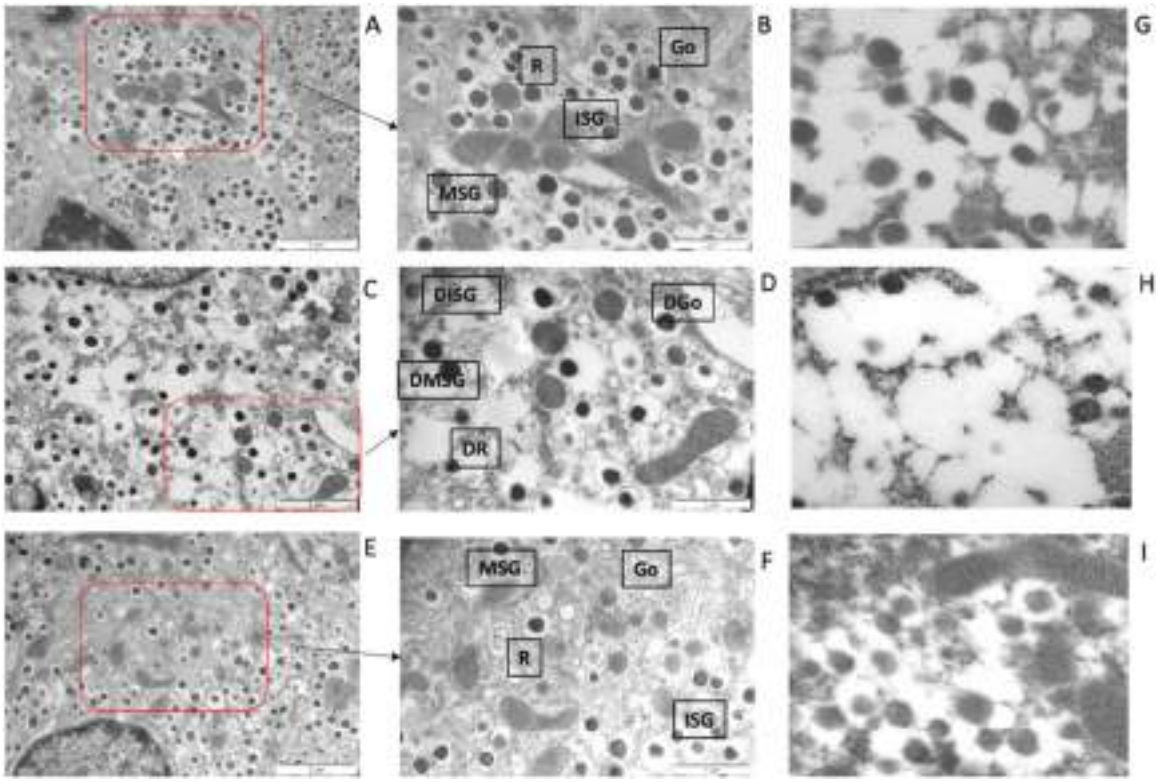

Fig. 5. Ultrastructural electron microscopy analysis of the pancreatic tissue. (A-B) β cells of healthy controls pancreas (20000X-60000X), showing endoplasmic reticulum (R), a Golgi apparatus (Go) and mature (MSG) and immature (ISG) secretory granules. (C-D) β cells of HFHFD pancreas (20000X-60000X), with short and dilated prophiles of dilated endoplasmic reticulum (DR) and Golgi cysternae (DGo) and numerous mature (DMSG) and scarce immature (ISG) dilated secretory granules. (E-F) β cells of pancreas from mice of the HFHFD + psilocybin group (20000X-60000X), with cysternae of endoplasmic reticulum (R), Golgi apparata (Go), numerous mature (MSG) and some immature (ISG) secretory granules. (G) β cells of ND pancreas (30000x), tagged with antibody anti-insulin (London White Resin embedded). (H) β cells of HFHFD pancreas (30000x), tagged with antibody anti-insulin (London White Resin embedded). (I) β cells of PSYLOCIN-treated pancreas (30000x), tagged with antibody anti-insulin (London White Resin embedded).

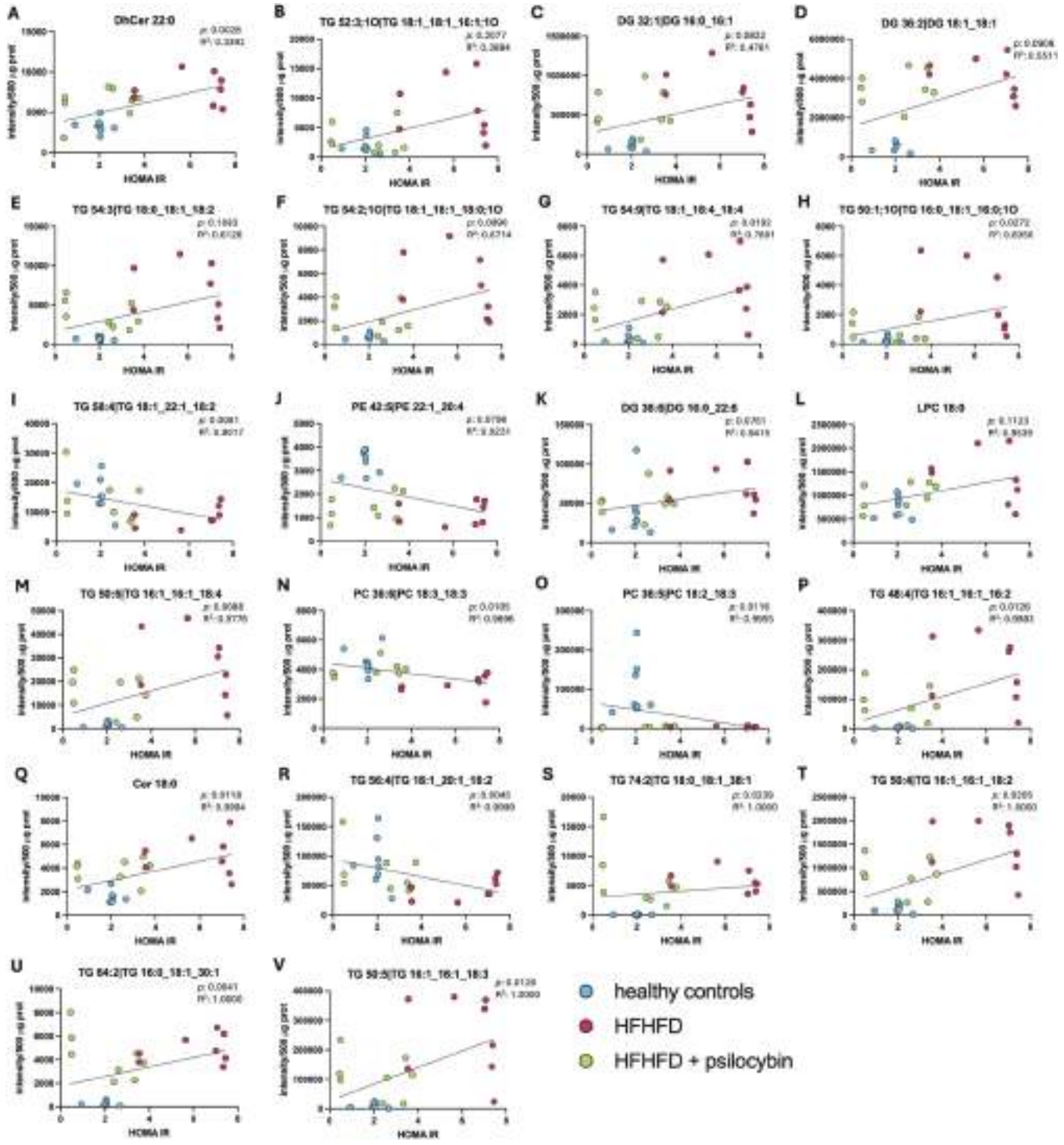

Fig. 6. Multivariate correlations between different hepatic lipid species from healthy control mice (light blue dots), HFHFD fed-mice (red dots), HFHFD mice treated with psilocybin (green dots) with HOMA-IR. The order of the panels follows the coefficient of determination (R^2). The x-axis shows HOMA-IR values, and the y-axis displays lipid peak intensity, normalized to protein concentration. (A) dihydroceramide 22:0; (B) oxidized triglyceride 52:3;1 O|18:1_18:1_16:1;1 O; (C) diglyceride 32:1|16:0_16:1; (D) diglyceride 36:2|DG 18:1_18:1; (E) triglyceride 54:3|18:0_18:1_18:2; (F) triglyceride 54:2;1 O|18:1_18:1_18:0;1 O; G triglyceride 54:9|18:1_18:4_18:4; (H) oxidized triglyceride 50:1;1 O|16:0_18:1_16:0;1 O; (I) triglyceride 58:4|18:1_22:1_18:2; (J) phosphatidylethanolamine 42:5|22:1_20:4; (K) diglyceride 38:6|16:0_22:6; (L) lysophosphatidylcholine 18:0; (M) triglyceride 50:6|16:1_16:1_18:4; (N) phosphatidylcholine 36:6|18:3_18:3; (O) phosphatidylcholine 36:5|18:2_18:3; (P) triglyceride 48:4|16:1_16:1_16:2; (Q) ceramide 18:0; (R) triglyceride 56:4|18:1_20:1_18:2; (S) triglyceride 74:2|18:0_18:1_38:1; (T) triglyceride 50:4|16:1_16:1_18:2; (U) triglyceride 64:2|16:0_18:1_30:1; (V) triglyceride 50:5|16:1_16:1_18:3. The correlations indicate that lipotoxic mediators (ceramides, DAGs, and mid-length TGs) track with higher HOMA-IR, whereas indices of fatty acid handling and membrane integrity (acylcarnitines, polyunsaturated PC/PE/plasmalogens, and very-long-chain PUFA-rich TGs) associate with lower HOMA-IR, consistent with a shift from storage/lipotoxic signaling toward oxidation and membrane-centric protection.

3.5. Low, nonpsychedelic doses of psilocybin reduce the HFHFD-associated muscular loss of function by a leptin-dependent mechanism

After demonstrating that psilocin significantly reduced the area of lipid droplets in an *in vitro* model of myosteatosis, indicating a direct effect of the drug on muscles (Fig. 7A-B), we performed a bulk RNAseq on the quadriceps, which revealed a robust transcriptomic regulation by both diet and treatment, as visualized by volcano plot (Fig. S8A). GSEA analysis was performed and displayed as lollipop plots of hallmark gene sets (Fig. S8B) which showed that psilocybin treatment upregulated the hallmark androgen response, downregulated by the HFHFD, while the opposite effects were observed in the hallmark fatty acid metabolism. The STRING network for GOBP Muscle System Process (Fig. 7D-E-F) showed that clusters of genes whose expression was significantly modified by HFHFD were normalized by psilocybin treatment. In detail, the GSVA of the bulk transcriptomic data of quadriceps revealed that psilocybin caused a significant increase in the gene sets related to the response to leptin (Fig. 7G-H). In agreement with leptin role in skeletal muscle (Fig. 7C), the gene sets responsible for lipase activity (Fig. 7I-J) and glucose import (Fig. 7K-L) were upregulated. HFHFD-fed mice treated with vehicle showed a significant reduction of the grid score (Fig. 8A); the time spent on the grid (Fig. 8B) and the time of the first fall (Fig. 8C) when compared to healthy controls. HFHFD-fed mice treated with psilocybin maintained better performances at the grid test

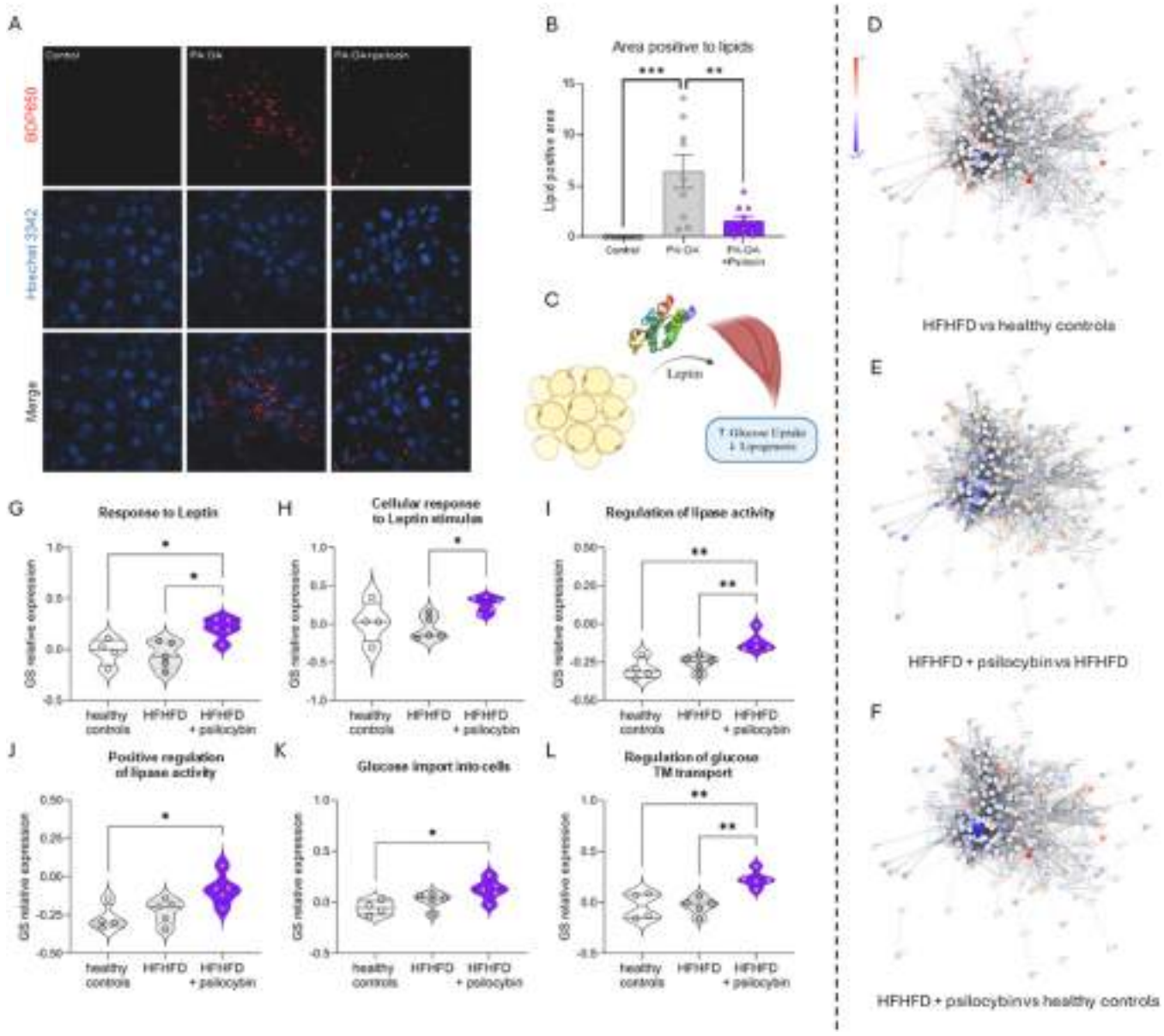

Fig. 7. Effect of psilocin in the C2C12-myosteatosis model and effect of psilocybin on leptin-dependent biological processes in quadriceps. (A-B) *In vitro* effect of psilocin on lipid accumulation in C2C12 differentiated myotubes. (A) LDs stained red with Bodipy and nuclei stained blue with Hoechst and (B) quantification of LDs are reported. Data are presented as mean ± S.E.M of three independent experiments analyzed in triplicate. **p < 0.01, ***p < 0.001. (C) Schematic representation of main pathways modulated by leptin in muscles. (D-F) STRING network representing the differentially expressed genes identified from the comparison of bulk RNAseq of muscular tissue of (D) HFHFD vs healthy controls, (E) HFHFD + psilocybin vs HFHFD, and (F) HFHFD + psilocybin vs healthy controls. The scalebar shows color mapping representing average log_2FC. (n = 5) (G-H) Violin plot representing leptin-related gene sets modulated by psilocybin treatment in muscular tissue, e.g. (G) response to leptin, (H) cellular response to leptin stimulus (n = 5). *p < 0.05. (I-J) Violin plot representing the effect of psilocybin in muscular gene sets involved in (I) lipase activity regulation and (J) positive regulation of lipase activity (n = 5). *p < 0.05, **p < 0.01. (K-L) Violin plot representing the effect of psilocybin in muscular gene sets of (K) glucose import and (L) regulation of glucose transmembrane (TM) transport (n = 5). *p < 0.05, **p < 0.01.

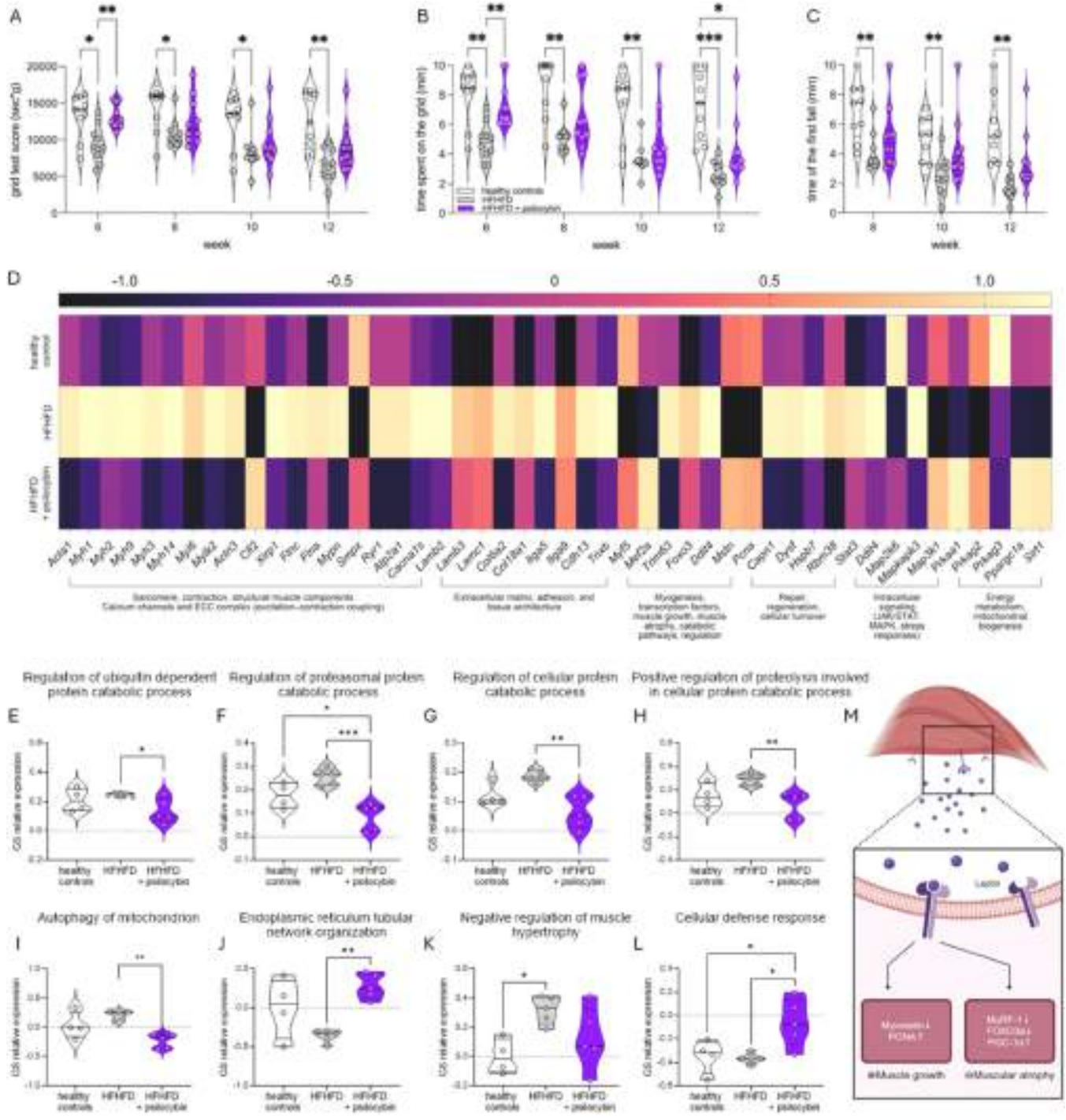

Fig. 8. Psilocybin effect on muscular performance and gene expression changes associated with muscle remodeling and atrophy. A-C Principal parameters evaluated during the grid test, performed after 6, 8, 10 and 12 weeks of pharmacological treatment, i.e., (A) total time spent on the grid normalized per animal body weight (score), (B) the time spent on the grid and (C) the time of the first fall from the grid. Data are presented as mean ± S.E.M. *$p < 0.05$, **$p < 0.01$, ***$p < 0.001$. (D) Heatmap chart of Z-score scaled gene expression of 48 genes significantly modified by psilocybin treatment. E-L Violin plot representing muscle gene sets modulated by psilocybin treatment, e.g. (E) regulation of ubiquitin dependent catabolic process, (F) regulation of proteasomal protein catabolic process, (G) regulation of cellular protein catabolic process, (H) positive regulation of proteolysis involved in cellular protein catabolic process, (I) autophagy of mitochondrion (J) endoplasmic reticulum tubular network organization, (H) negative regulation of muscle hypertrophy and (L) cellular defense response ($n = 5$). *$p < 0.05$, **$p < 0.01$, ***$p < 0.001$. (M) Schematic representation of muscle remodeling gene expression modulated by leptin.

compared to HFHFD-fed vehicle-treated mice. Moreover, psilocybin fully restored the expression of diet-downregulated genes encoding adenosine monophosphate-activated protein kinase (AMPK) subunits (Prkaa1, Prkag2, Prkag3), sirtuin1 (Sirt1) and peroxisome proliferator-activated receptor gamma coactivator 1-alpha (Ppargc1a). HFHFD also increased the atrophy-related marker tripartite motif containing 63 (Trim63) gene expression (encoding for muscle RING finger 1; MuRF-1), while psilocybin significantly reduced it. In parallel, psilocybin upregulated proliferating cell nuclear antigen (Pcna), myostatin (Mstn) and myocyte enhancer factor 2 A (Mef2a), which were all suppressed by

HFHFD, with Mef2a exceeding control levels (Fig. 8D). These effects are consistent with the physiological actions promoted by leptin (Fig. 8M). Gene-set analyses showed that psilocybin reversed HFHFD-induced alterations in GOBP pathways related to polysaccharide (HFHFD vs. HFHFD + psilocybin $p < 0.05$; Fig. S9A) and cholesterol metabolism (healthy controls vs. HFHFD + psilocybin $p < 0.01$; Fig. S9B), protein catabolism and proteolysis (Fig. 8E-H), mitochondrial autophagy, organization of the tubular endoplasmic reticulum, hypertrophy and cellular stress responses (Fig. 8I-L). Overall, it's possible to conclude that psilocybin restored both metabolic and structural transcriptional programs disrupted by HFHFD.

3.6. Psilocin reduces lipid accumulation in human hepatic cell lines by a 5-HT2A-independent, 5-HT2B-dependent mechanism

Since the well-known central effects of psilocybin are mediated by the 5-HT2A receptor, the involvement of this isoform in the metabolic effects observed *in vivo* was evaluated in HepG2 cells where a loss of function mutation of the 5-HT2A receptor was induced by the CRISPR/Cas9 technique (Fig. 9A), incubated with a fatty acid mixture to induce lipid accumulation. HepG2 cells with mutant 5-HT2AR were still responsive to the anti-steatotic action of psilocin, as indicated by the reduction of lipid positive area compared to cells treated with the PA:OA mix (Fig. 9B for images, Fig. 9C for quantification, concentration-effect effect reported in Fig. S10), excluding the role of 5-HT2A in psilocin metabolic effect. We then evaluated the functional activity of psilocin on the three 5-HT2 isoforms, demonstrating that psilocin is a 5-HT2A/2 C partial agonist, as expected, but is surprisingly devoid of 5-HT2B agonist activity (Fig. 9D). Even more of note, psilocin exerts a marked antagonistic activity on 5-HT2B (Fig. 9E). Further *in vitro* studies performed on HepG2 cells incubated with the fatty acid mixture, revealed that the anti-steatotic effect of psilocin was virtually identical to that exerted by the 5-HT2B selective antagonist RS-127445 (Fig. 9F for images, Fig. 4G for quantification). The pivotal role of 5-HT2B in the anti-steatotic effect of psilocin was also confirmed in another cellular model of lipid accumulation, obtained with human hepatoma HUH-7 cells (Fig. S11).

4. Discussion

We demonstrated here that the chronic administration of low-nonpsychedelic doses of psilocybin improves metabolic abnormalities induced by the administration to C57BL6/J male mice of a diet rich in fat and fructose, a widely-used experimental model of metabolic dysfunctions [42,64,65]. Behavioral tests excluded CNS toxicity and suggested a potential reduction of anxiety, a condition often associated to metabolic diseases, together with other mental disorders [66–68]. Total food intake was not significantly modified by the treatment. However, we did not assess reward seeking behaviors, such as food craving or alcohol preference, which could be explored in future studies to assess any potential effects on motivational pathways.

Psilocybin caused a dramatic improvement of liver steatosis, as demonstrated by histological, biochemical and untargeted lipidomic analyses. The impact of psilocybin on hepatic lipids was also evident from bulk transcriptomic results of liver tissue. GSVA analysis showed that gene sets related to lipids (localization, storage, import and translocation, according to the gene ontology analysis, biological processes) were altered in HFHFD-fed mice and normalized by psilocybin treatment. One of the genes mainly influenced by psilocybin treatment was *Cidea*. This protein from the Cell death-inducing DFF45-like effector (CIDE) family [69], is a fundamental regulator of lipid storage by playing a crucial role in the fusion and growth of lipid droplets (LDs). The strong downregulation of *Cidea* and the expression modifications of its network induced by psilocybin, as evidenced by the STRING plots (Fig. 2I-J-K), are consistent with the observed antilipogenic and anti-steatotic effects of this drug, since Cidea is localized to LD-LD contact domains, and promotes lipid exchange and storage in the hepatocytes containing large LDs [70]. The increase of lipid amount in the liver, hallmark of MASLD, is due to increased hepatic lipid uptake and synthesis [71]. Hepatic lipidome analysis showed a significant reduction of triglycerides and oxidized triglycerides, since over two-thirds of the total identified triglycerides, and nearly all (20/23) of the oxidized triglycerides, were significantly reduced after treatment. The oxidation of hepatic fatty acids normally acts as an adaptive response to lipid overload, to reduce intracellular triglyceride accumulation and prevent lipotoxicity. However, in MASLD, where this process is chronically upregulated or overloaded, it might contribute to oxidative stress and hepatocellular damage, promoting disease progression [72]. The accumulation of unsaturated triglycerides in HFHFD mice may be attributed to a protective mechanism in which unsaturated fatty acids are stored in triglycerides to protect the liver from SFA-induced lipotoxicity [73]. Regarding the other lipids modified by the treatment, the increase of phosphatidylcholine is consistent with its role in the liver where, particularly in overnutrition, reduced phospholipid levels have been implicated in the development of MASLD [74]. Palmitoleic acid (16:1), one of the free fatty acids reduced after treatment, has been proposed as a lipid biomarker of FA synthesis and of hepatic lipogenesis [75]; the effect of psilocybin treatment on its hepatic amount suggests a possible modulation of the cellular pathways involved in *de novo* lipogenesis, potentially reflecting improved metabolic homeostasis and reduced hepatic lipid accumulation. Furthermore, lipidomic data evidence that DAG and ceramide species coexist also in a physiological setting, suggesting that even in healthy liver, variability in insulin sensitivity is modulated by lipid mediators known to impair insulin receptor signaling through Protein Kinase C epsilon (PKCε) activation and Akt inhibition, respectively [76]. In HFHFD mice, a pattern consistent with diet-induced hepatic insulin resistance was evident, where ceramide accumulation and sterol ester metabolism synergize to disrupt insulin signaling, while altered TG composition reflects excessive lipid storage and impaired turnover. Psilocybin treatment was associated to the presence of long-chain polyunsaturated phospholipids in the liver, suggesting a partial restoration of membrane fluidity and receptor microdomain organization, potentially counterbalancing the ceramide-mediated defects of the HFHFD model. Notably, the appearance of DhCer 22:0, a very-long-chain, fully saturated specie, may reflect ongoing sphingolipid remodeling, which in some contexts is associated with less potent inhibition of Akt compared to shorter-chain ceramides [77]. Collectively, these data indicate a progressive shift in lipid predictors of HOMA-IR from the DAG- and ceramide-enriched but balanced network observed in healthy controls, to a sterol- and TG-loaded, ceramide-dominant profile in HFHFD, and finally to a psilocybin-induced state, characterized by increased membrane unsaturation. This suggests that psilocybin can remodel the hepatic lipidome to favor a membrane microenvironment more permissive to insulin signaling.

The GSEA analysis of the hallmarks of cancer points at fatty acid metabolism, hypoxia, mTorc1-signaling, and epithelial to mesenchymal transition as fundamental processes regulated by the drug. Besides downregulating the genes involved in fatty acid metabolism, psilocybin had the same effect on the other gene sets, suggesting an intriguing pleiotropic action on the steatotic liver. mTORC1 signaling plays a pivotal role in regulating hepatic lipid metabolism, since its activation promotes lipogenesis and inhibits lipophagy [78], with a putative role in obesity-related insulin resistance. Moreover, hypoxia and epithelial to mesenchymal transition are processes involved in the evolution of MASLD and metabolic dysfunction-associated steatohepatitis (MASH) to hepatocellular carcinoma (HCC), a tumor fostered by the positive energy balance of the lipid-rich liver [79]. Taken together, these observations suggest that the metabolic effects of psilocybin may primarily be hepatic, and it tempting to hypothesize that psilocybin could reduce the risk of MASLD/MASH-driven HCC by inhibiting cancer-related mechanisms. To expand the translational value of these results, we attempted to further investigate the molecular mechanism of psilocybin in the

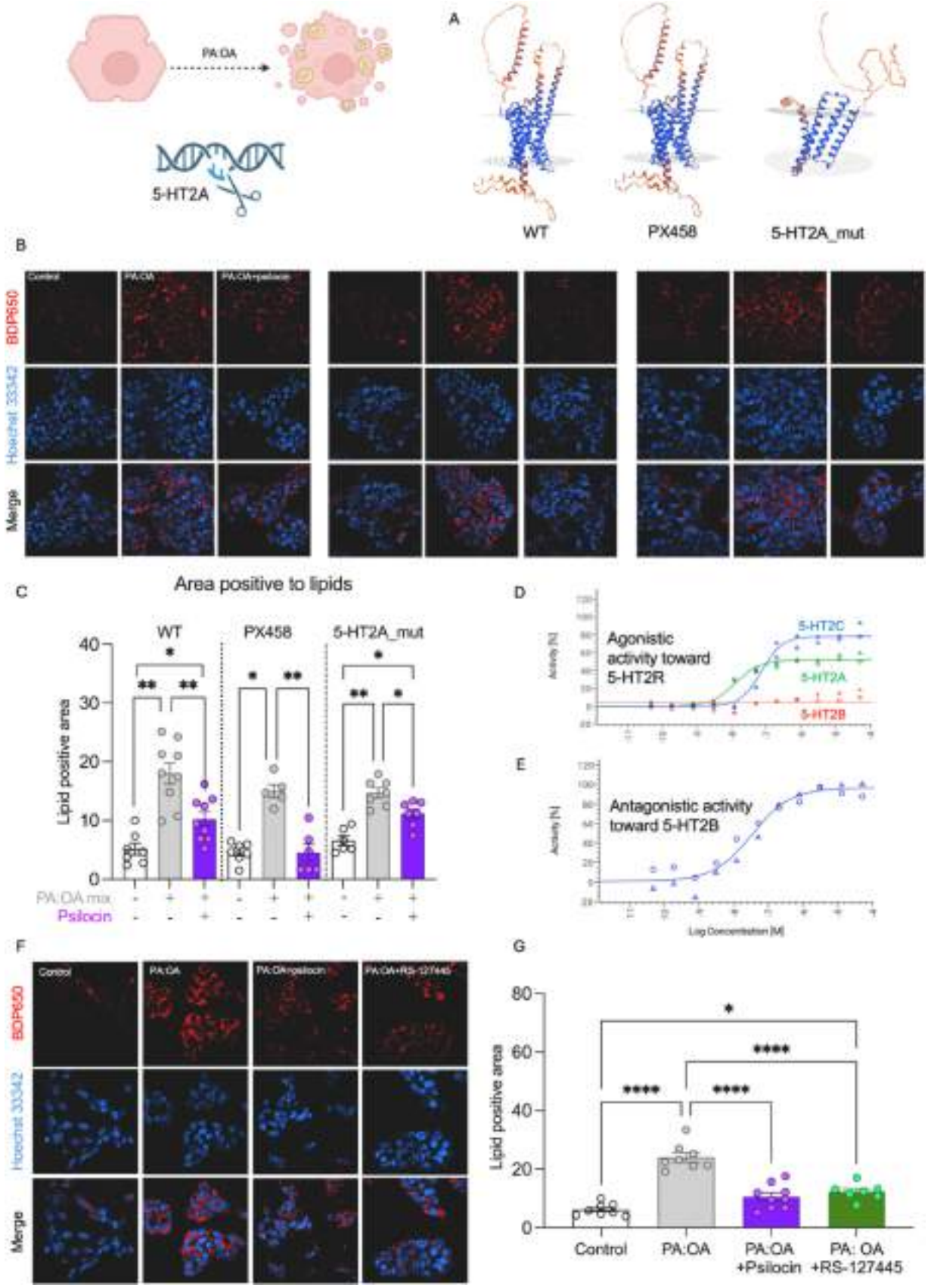

(caption on next page)

Fig. 9. Molecular mechanism of action of Psilocin at 5-HT2 Receptors. A Predicted protein structure of 5HT2A receptor in WT, PX458 and 5-HT2A_mut cells (https://swissmodel.expasy.org/) based on SANGER sequencing. B Effect of loss of 5-HT2A function on lipid droplets formation. LDs stained red with Bodipy and nuclei on WT (left panels), PX458 (middle panels) and 5HT2A_mut (right panel) cells stained blue with Hoechst. C Quantification of lipid accumulation (lipid positive area normalized on cell number). Data are presented as mean ± S.E.M. of three independent experiments each performed in triplicate. *$p < 0.05$, **$p < 0.01$. D Agonist activity of psilocin at the human 5-HT2A (curves in green), 5-HT2B (curves in red) and 5-HT2C (curves in blue) receptors expressed in CHO cells. E Antagonist activity of psilocin at the human 5-HT2B receptor expressed in CHO cells F Effect of 5-HT2B antagonism on lipid droplets formation. G Quantification of lipid accumulation (lipid positive area normalized on cell number). Data are presented as mean ± S.E.M. of three independent experiments each performed in triplicate. *$p < 0.05$, ****$p < 0.0001$.

liver. We demonstrated that, besides the well-known partial agonism to 5-HT2AR responsible for central psychedelic effects [80], and 5-HT2CR, psilocin is also a 5-HT2BR antagonist. The *in vitro* models of liver steatosis obtained by incubating HepG2 and HUH7 cells with a mixture of fatty acids and tested with combined use of pharmacological inhibition and genetic modification lead us to the hypothesis that psilocybin has a direct effect on lipid accumulation in hepatic cells thanks to its 5-HT2B antagonism. A role of 5-HT2CR agonism in psilocin metabolic actions cannot be excluded, since the 5-HT2CR agonist lorcaserin was approved by the FDA for obesity treatment in 2012. Notably, lorcaserin was withdrawn from the market in 2020 due to safety concerns about an increased risk of cancer. Lorcanserin is also a partial agonist of 5-HT2B, a feature in common with the drug pergolide, also withdrawn from the market, due to causal relationship with cardiac valvulopathy [6]. The high affinity of psilocybin for 5-HT2BR has prompted caution when considering chronic psilocybin treatment because of the known association between 5-HT2BR agonism and the risk for cardiac valvulopathy. We here demonstrated for the first time by FLIPR experiments that psilocin is not an agonist at 5-HT2B receptors (Fig. 4D), in contrast with serotonin, lorcaserin and pergolide, providing reassurance over concerns about some of the potential risks of chronic psilocybin therapy (Fig. S12). Additionally, our *in vitro* experiments demonstrated that psilocin is an antagonist of 5-HT2B receptor (Fig. 4E). This antagonistic effect may potentially have protective effect against 5-HT2BR activation-induced fibrosis in different organs, including liver and cardiac valves worthwhile of further exploration. These results are in line with previous observations which demonstrated that the inhibition of 5-HT2BR, whose expression is increased in obese mice and humans and correlates with metabolic dysfunction, reduces lipolysis in visceral adipocytes and improves obesity-associated insulin resistance [81]. These findings, obtained either by genetic deletion or pharmacological blockade of this receptor in high-fat diet-fed mice, are consistent with our results, pointing at 5-HT2B signaling as a potential therapeutic target for metabolic diseases.

In the liver, we also demonstrated an increase of hepatic glycogen in HFHFD-treated mice, which is consistent with preclinical and clinical observations in MASLD models and in patients [82,83]. Glycogen accumulation is reduced by psilocybin, in accordance with the expression of the Akt, that is known to promote glycogen synthesis in response to increased glucose uptake in the liver by the disinhibition of the enzyme glycogen synthase [84]. Akt has a pivotal role in the cellular signaling pathways connecting insulin and lipid metabolism [85]. As suggested by the normalization of insulin substrate receptor 1 (Irs1) expression, psilocybin may also restore insulin signaling in the liver [86,87]. Moreover, also increased hepatic Akt1 phosphorylation likely supports improved metabolic homeostasis by improving insulin signaling, enhancing hepatocellular survival mechanisms, and attenuating inflammatory and fibrotic responses that may drive disease progression. This is consistent with its effect on hepatic lipidome, i.e., a shift from the ceramide- and membrane-perturbed state induced by HFHFD to a condition enriched in protective membrane lipids and shorter-chain TGs, consistent with the observed histological and biochemical improvements in liver steatosis and glucose homeostasis.

Psilocybin displays potent effects on glucose homeostasis as shown in the ipGTT test, where blood glucose and insulin, both abnormally high in HFHFD-treated mice, were reduced by the treatment, which markedly reduced glucose and insulin AUC (area under the curve), virtually identical to those seen in healthy control mice. HFHFD mice were severely insulin resistant as shown by HOMA-IR values, and psilocybin substantially normalized this index. Consistently, psilocybin showed normalizing effects on beta cell ultrastructure and insulin containing secretory granules, as shown by electron microscopy and on the production of pancreatic hormones. Since insulin resistance, besides being a disorder *per se*, is also a recognized trigger for liver steatosis [88,89], the pleiotropic effects of psilocybin in this regard deserve further attention, also considering the urgent need of medications for MASLD. In this context, it is worth noting that glucose-dependent insulinotropic polypeptide (GIP) was increased by HFHFD and normalized by psilocybin. Dual GLP-1/GIP agonism is the pharmacological mechanism of the most recent drug gaining approval for obesity, i.e., tirzepatide [90]. Interestingly, a paracrine interplay between serotonin and GIP has been demonstrated in the regulation of gut function [91], further indicating the existence of a functional axis between incretins and serotonin, possibly modulated by psilocybin action with potential therapeutic fallouts on glucose and lipid metabolism.

The circulating levels of the two adipokines resistin and leptin, which are both increased by HFHFD diet are normalized by psilocybin treatment. Their mutual relationship acts at the central level, and resistance to leptin and resistin, present in HFHFD mice, is pivotal in driving metabolic and cardiovascular complications [92]. The psilocybin effects on leptin resistance depict an intriguing scenario, especially by analyzing its action on skeletal muscle. From a functional point of view, HFHFD leads to a deterioration of muscular function, which is a common complication of obesity, diabetes and MASLD [93], and psilocybin treatment reduced and delayed this effect. In quadriceps, psilocybin restored the AMPK–SIRT1–PGC-1α axis, a central regulatory module controlling mitochondrial biogenesis, substrate utilization, and protection against muscle atrophy. AMPK is a primary upstream activator of PGC-1α, while SIRT1 provides an additional layer of control over muscle growth, differentiation and lipid–glucose handling. This axis is typically blunted under obesity-associated metabolic stress, resulting in reduced metabolic flexibility [94]. The marked HFHFD-induced suppression of Prkaa1, Prkag2, Prkag3, Sirt1 and Ppargc1a observed in our model is consistent with this phenomenon [95], and their full normalization by psilocybin indicates a reactivation of core metabolic regulatory programs. In parallel, the reduction of Trim63 expression and the enhancement of growth-related markers (Pcna, Mstn) highlight a shift toward an anti-atrophic, pro-anabolic state. These effects align with the normalization of leptin-related pathways, which further support muscle maintenance and oppose catabolic signaling [96]. The pronounced upregulation of Mef2a further supports a recovery of regenerative programs normally impaired by HFHFD [97]. Together, these findings indicate that psilocybin counteracts key metabolic and structural impairments in skeletal muscle by re-engaging core energy-sensing and growth-regulatory circuits, ultimately restoring a more adaptive transcriptional state. From a mechanistic point of view, transcriptomic data of quadriceps clearly indicate that a significant increase of the cellular responses to leptin and to androgens was observed in psilocybin-treated mice, with a consequent increase of glucose uptake (and reduction of insulin resistance) and a reduction in the expression of lipogenic genes. It is known that the androgen response in muscle is impaired in metabolic diseases, and this can inhibit muscle function and the effective production of energy [98,99], since androgen signaling in skeletal muscle plays a pivotal role in the regulation of metabolic and contractile

functions [100]. An excess of circulating leptin, as observed in the HFHFD-fed mice of this study and clinically in patients with obesity or other metabolic diseases [33], can lead to a reduction of androgens and androgen signaling in muscle cells [101]. Leptin has an impact on muscle morphology and function in the elderly and patients with obesity and diabetes [102]. By demonstrating that psilocybin has a leptin-specific effect both in the liver and in muscle, we would like to suggest that psilocybin may act also as a leptin sensitizer, to induce its positive metabolic effects [103].

Notably, other researchers experimenting with higher doses of psilocybin for very short periods in different models of obesity did not show body weight effects [17,18], potentially signaling the importance of chronic low dose treatment in ameliorating HFHFD induced metabolic dysfunction, also considering that previous observations by Huang and collaborators reported a reduction of body weight increase in rats fed with "cafeteria diet" treated for 27 days with 0.1 or 5 mg/kg i.p. psilocybin [16].

It is worth mentioning that we have recently completed a Phase I study to assess pharmacokinetics and tolerability of low, single ascending doses of psilocybin (0.5–2 mg), confirming that there are no CNS detrimental effects in healthy normal weight and obese subjects (data not shown).

We here demonstrated that low dose chronic psilocybin exerts beneficial actions on lipid and carbohydrate metabolism in the liver, with significant reductions in body weight increase, insulin resistance and hepatic steatosis. A limitation to the generalizability of the study is that it did not consider gender/sex issues, since all experiments were conducted in male mice and the present findings may not fully reflect responses in females, which can exhibit different metabolic and hormonal profiles. Furthermore, we did not analyze body mass composition. However, preliminary results obtained in adipocytes' spheroids suggest a direct effect on psilocybin also on the adipose tissue (Fig. S13).

Moreover, our results indicate that these effects are due to 5-HT2BR antagonism and involve the restoration of leptin sensitivity, in the liver and skeletal muscle. A mutual connection between responses to leptin and the 5-HT2B receptors has been suggested in the past, although limited to the central regulation of energy expenditure [104]. Moreover, a recent paper clearly demonstrated that peripheral serotonin signaling impairs insulin sensitivity and energy metabolism in skeletal muscle right through the 5-HT2B receptor, since muscle-specific 5-ht2br deletion in HFD-fed mice improved glucose tolerance, insulin sensitivity, and metabolic health, while the pharmacological inhibition of 5-HT2B in muscle cells restored insulin sensitivity [105].

The involvement of 5-HT2RC cannot be excluded also in this regard, since 5-HT2CR knock-out mice with leptin overexpression showed an exacerbation of obesity [106]. On these bases, the observed effects of psilocybin on leptin signaling may be partially ascribed also to a 5-HT2CR-mediated leptin sensibilization, which is beneficial for both metabolic dysfunctions and muscular function.

In summary, we demonstrated that the 5-HT2BR-mediated beneficial metabolic effects induced by non-psychedelic psilocybin are correlated to a remodeling of the hepatic lipidome and accompanied by preservation of muscular strength and function in mice. These effects taken alltogether, point to psilocybin as a potential muscle-sparing, CNS- and cardio-safe drug candidate for the treatment of MASLD, obesity and type 2 diabetes mellitus.

Funding

This work was supported by MGGM Therapeutics Inc. and by the Italian Ministry of University and Research (MUR), grant PON 2014–2020 "Research and Innovation" resources—Green/Innovation Action—DM MUR 1062/2021—for the research EPAGREEN".

CRediT authorship contribution statement

Camillo Morano: Writing – review & editing. **Daniela Gabbia:** Writing – original draft, Visualization, Validation, Methodology, Investigation, Formal analysis. **Stefano La Rosa:** Resources, Methodology. **Martina Colognesi:** Writing – original draft, Visualization, Investigation, Formal analysis. **Michele Dei Cas:** Methodology, Investigation. **Miles Sarill:** Writing – original draft, Validation, Methodology, Investigation, Formal analysis, Data curation. **Rita Clara Paroni:** Supervision, Resources, Methodology, Investigation, Data curation. **Anna Signor:** Visualization, Investigation. **Andrea Rinaldi:** Methodology, Investigation, Formal analysis, Data curation. **Giuseppe Daniele:** Visualization, Formal analysis. **Lucia Centofanti:** Writing – original draft, Visualization, Methodology, Formal analysis. **Luciano Cascione:** Software, Investigation, Formal analysis, Data curation. **Miriam Saponaro:** Writing – original draft, Validation, Methodology, Investigation, Formal analysis, Data curation. **Maria Elena Lunati:** Writing – review & editing, Resources. **Loredana Bucciarelli:** Writing – review & editing, Resources. **Ilaria Goggi:** Investigation. **Giulia Guarato:** Methodology, Investigation. **Diana Pendin:** Supervision. **Sonia Sonda:** Validation, Formal analysis. **Stefano Comai:** Resources, Data curation. **Ilaria Zanotto:** Investigation. **Abdullah Alajati:** Supervision, Resources. **Gianfranco Pasut:** Writing – review & editing, Resources. **Marco Pappagallo:** Resources. **Marco Gentilucci:** Resources. **Franco Folli:** Writing – review & editing, Supervision, Resources, Project administration, Conceptualization. **Marco Banzato:** Investigation. **Andrea Alimonti:** Supervision, Resources. **Sara Nunziata:** Investigation. **Sara De Martin:** Writing – review & editing, Writing – original draft, Visualization, Supervision, Project administration, Funding acquisition, Data curation, Conceptualization. **Giovanna Finzi:** Methodology, Investigation. **Manfredi Paolo L:** Writing – review & editing, Project administration, Conceptualization. **Andrea Mattarei:** Writing – review & editing, Supervision, Resources, Methodology.

Declaration of Generative AI and AI-assisted technologies in the writing process

During the preparation of this work the authors used ChatGPT to revise English language and syntax. After using this tool, the authors reviewed and edited the content as needed and takes full responsibility for the content of the publication.

Declaration of Competing Interest

MC, DG, MB, SC, SDM, AM, MP, PLM, FF, GP, AAla are employed by institutions that received funds from Relmada Therapeutics or from companies affiliated with Relmada Therapeutics or received personal fees from Relmada Therapeutics and or MGGM LLC. MP holds stock ownership with Acadia, and received personal fees from Overlook Medical Center. SDM, AM, MP, FF and PLM are co-inventors on patents related to psilocybin. The other authors have no conflicts of interest.

Acknowledgments

We would like to thank and remember with deep gratitude Prof. Genny Orso for her useful support in the Crispr/Cas9 experiments. The scientific support from the CRIETT center of University of Insubria (instrument code MIC01) is greatly acknowledged.

Appendix A. Supporting information

Supplementary data associated with this article can be found in the online version at doi:10.1016/j.phrs.2025.108080.

Data availability

Data will be made available on request.

References

[1] R. Von Rotz, et al., Single-dose psilocybin-assisted therapy in major depressive disorder: a placebo-controlled, double-blind, randomised clinical trial, eClinicalMedicine 56 (2023) 101809.
[2] N.C. Borgogna, et al., Incremental efficacy systematic review and meta-analysis of psilocybin-for-depression RCTs, published online ahead of print: April 23,, Psychopharmacology (2025), https://doi.org/10.1007/s00213-025-06788-w. published online ahead of print: April 23,.
[3] S. Meshkat, et al., Psilocybin-Assisted Psychotherapy for Treatment-Resistant Depression in Bipolar II Disorder, Psychedelic Med. 3 (1) (2025) 53–58.
[4] L. Seillier, et al., Psilocybin has a narrow therapeutic window as an antidepressant treatment, Prog. NeuroPsychopharmacol. Biol. Psychiatry 138 (2025) 111368.
[5] T. Anderson, et al., Microdosing psychedelics: personality, mental health, and creativity differences in microdosers, Psychopharmacology 236 (2) (2019) 731–740.
[6] K.P. Kuypers, et al., Microdosing psychedelics: More questions than answers? An overview and suggestions for future research, J. Psychopharmacol. 33 (9) (2019) 1039–1057.
[7] V. Polito, R.J. Stevenson, A systematic study of microdosing psychedelics, PLoS ONE 14 (2) (2019) e0211023.
[8] L.P. Cameron, A. Nazarian, D.E. Olson, Psychedelic Microdosing: Prevalence and Subjective Effects, J. Psychoact. Drugs 52 (2) (2020) 113–122.
[9] D. Rosenbaum, et al., Microdosing psychedelics: Demographics, practices, and psychiatric comorbidities, J. Psychopharmacol. 34 (6) (2020) 612–622.
[10] C. Ly, et al., Psychedelics Promote Structural and Functional Neural Plasticity, Cell Rep. 23 (11) (2018) 3170–3182.
[11] S. Sonda, et al., Emerging mechanisms of psilocybin-induced neuroplasticity, Trends Pharmacol. Sci. 46 (11) (2025) 1130–1143.
[12] M.K. Madsen, et al., Psychedelic effects of psilocybin correlate with serotonin 2A receptor occupancy and plasma psilocin levels, Neuropsychopharmacol 44 (7) (2019) 1328–1334.
[13] I. Moutkine, et al., Heterodimers of serotonin receptor subtypes 2 are driven by 5-HT2C protomers, J. Biol. Chem. 292 (15) (2017) 6352–6368.
[14] A.B. Wulff, C.D. Nichols, S.M. Thompson, Preclinical perspectives on the mechanisms underlying the therapeutic actions of psilocybin in psychiatric disorders, Neuropharmacology 231 (2023) 109504.
[15] M. Berger, J.A. Gray, B.L. Roth, The Expanded Biology of Serotonin, Annu Rev. Med 60 (1) (2009) 355–366.
[16] J. Huang, et al., Chronic Treatment With Psilocybin Decreases Changes in Body Weight in a Rodent Model of Obesity, Front Psychiatry 13 (2022) 891512.
[17] N. Fadahunsi, et al., Acute and long-term effects of psilocybin on energy balance and feeding behavior in mice, Transl. Psychiatry 12 (1) (2022) 330.
[18] J. Shakir, et al., Effects of psilocybin on body weight, body composition, and metabolites in male and female mice, Physiol. Behav. 284 (2024) 114627.
[19] A. Antonini, W. Poewe, Fibrotic heart-valve reactions to dopamine-agonist treatment in Parkinson's disease, Lancet Neurol. 6 (9) (2007) 826–829.
[20] M. Israelsen, et al., Steatotic liver disease, Lancet 404 (10464) (2024) 1761–1778.
[21] M.E. Rinella, et al., A multi-society Delphi consensus statement on new fatty liver disease nomenclature, J. Hepatol. 0 (0) (2023), https://doi.org/10.1016/j.jhep.2023.06.003.
[22] M. Bignotto, et al., Synergistic effects of glucose tolerance and BMI on cardiovascular events and all-cause mortality in a healthy population: CA.ME.LI. A study 7 years follow-up, Am. J. Physiol. Endocrinol. Metab. 327 (4) (2024) E498–E511.
[23] E.A. Bohula, et al., Cardiovascular Safety of Lorcaserin in Overweight or Obese Patients, N. Engl. J. Med 379 (12) (2018) 1107–1117.
[24] J. Namkung, H. Kim, S. Park, Peripheral Serotonin: a New Player in Systemic Energy Homeostasis, Mol. Cells 38 (12) (2015) 1023–1028.
[25] C.-M. Oh, et al., Regulation of systemic energy homeostasis by serotonin in adipose tissues, Nat. Commun. 6 (1) (2015) 6794.
[26] C.-M. Oh, S. Park, H. Kim, Serotonin as a New Therapeutic Target for Diabetes Mellitus and Obesity, Diabetes Metab. J. 40 (2) (2016) 89.
[27] J.M. Yabut, et al., Emerging Roles for Serotonin in Regulating Metabolism: New Implications for an Ancient Molecule, Endocr. Rev. 40 (4) (2019) 1092–1107.
[28] K.J. Suchacki, et al., The serotonin transporter sustains human brown adipose tissue thermogenesis, Nat. Metab. 5 (8) (2023) 1319–1336.
[29] C.M. Prado, et al., Sarcopenic obesity in older adults: a clinical overview, Nat. Rev. Endocrinol. 20 (5) (2024) 261–277.
[30] M.E. Cleasby, P.M. Jamieson, P.J. Atherton, Insulin resistance and sarcopenia: mechanistic links between common co-morbidities, J. Endocrinol. 229 (2) (2016) R67–R81.
[31] Z.-Y. Yang, W.-L. Chen, Examining the Association Between Serum Leptin and Sarcopenic Obesity, JIR 14 (2021) 3481–3487.
[32] S. Russo, et al., Meta-Inflammation and Metabolic Reprogramming of Macrophages in Diabetes and Obesity: The Importance of Metabolites, Front Immunol. 12 (2021) 746151.
[33] R. Ter Horst, et al., Sex-Specific Regulation of Inflammation and Metabolic Syndrome in Obesity, ATVB 40 (7) (2020) 1787–1800.
[34] M. Longo, et al., DGAT1 and DGAT2 Inhibitors for Metabolic Dysfunction-Associated Steatotic Liver Disease (MASLD) Management: Benefits for Their Single or Combined Application, IJMS 25 (16) (2024) 9074.
[35] Y. Frion-Herrera, et al., Oleocanthalic acid improves MASH features via a NOX1-dependent mechanism, Eur. J. Pharmacol. 1002 (2025) 177847.
[36] M. Ricchi, et al., Differential effect of oleic and palmitic acid on lipid accumulation and apoptosis in cultured hepatocytes, J. Gastro Hepatol. 24 (5) (2009) 830–840.
[37] Z. Heidari, et al., Impact of Tissue Factor Gene Knockout on Coagulation Properties of Umbilical Cord-Derived Multipotent Mesenchymal Stromal/Stem Cells, Cell Biochem. amp Funct. 42 (8) (2024) e70021.
[38] M. Saponaro, et al., CDCP1 expression is frequently increased in aggressive urothelial carcinoma and promotes urothelial tumor progression, Sci. Rep. 13 (1) (2023) 73.
[39] Y. Frion-Herrera, et al., Oleocanthalic acid improves MASH features via a NOX1-dependent mechanism, Eur. J. Pharmacol. 1002 (2025) 177847.
[40] Q. Zhang, et al., Mangiferin Improved Palmitate-Induced-Insulin Resistance by Promoting Free Fatty Acid Metabolism in HepG2 and C2C12 Cells via PPAR α: Mangiferin Improved Insulin Resistance, J. Diabetes Res. 2019 (2019) 1–13.
[41] T. Alquier, V. Poitout, Considerations and guidelines for mouse metabolic phenotyping in diabetes research, Diabetologia 61 (3) (2018) 526–538.
[42] M. Vacca, et al., An unbiased ranking of murine dietary models based on their proximity to human metabolic dysfunction-associated steatotic liver disease (MASLD), Nat. Metab. 6 (6) (2024) 1178–1196.
[43] B.-T. Zhang, et al., Obesity and cancer: Mouse models used in studies, Front Oncol. 13 (2023) 1125178.
[44] H. Shi, et al., Different Types of Dietary Fat and Fructose Interactions Result in Distinct Metabolic Phenotypes in Male Mice, J. Nutr. Biochem. 111 (2023) 109189.
[45] T.D.R. Lima, et al., High-fat diet and fructose drink introduced after weaning rats, induces a better human obesity model than very high-fat diet, J. Food Biochem 45 (4) (2021), https://doi.org/10.1111/jfbc.13671.
[46] D. Gabbia, et al., The phenolic compounds tyrosol and hydroxytyrosol counteract liver fibrogenesis via the transcriptional modulation of NADPH oxidases and oxidative stress-related miRNAs, Biomed. Pharmacother. 157 (2023), https://doi.org/10.1016/j.biopha.2022.114014.
[47] D. Gabbia, et al., Tyrosol attenuates NASH features by reprogramming the hepatic immune milieu, Eur. J. Pharmacol. 969 (2024) 176453.
[48] R. Guardado-Mendoza, et al., Pancreatic islet amyloidosis, β-cell apoptosis, and α-cell proliferation are determinants of islet remodeling in type-2 diabetic baboons, Proc. Natl. Acad. Sci. USA 106 (33) (2009) 13992–13997.
[49] T.V. Fiorentino, et al., Exenatide regulates pancreatic islet integrity and insulin sensitivity in the nonhuman primate baboon Papio hamadryas, JCI Insight 4 (20) (2019) e93091.
[50] A.M. Bolger, M. Lohse, B. Usadel, Trimmomatic: a flexible trimmer for Illumina sequence data, Bioinformatics 30 (15) (2014) 2114–2120.
[51] A. Dobin, et al., STAR: ultrafast universal RNA-seq aligner, Bioinformatics 29 (1) (2013) 15–21.
[52] S. Anders, P.T. Pyl, W. Huber, HTSeq—a Python framework to work with high-throughput sequencing data, Bioinformatics 31 (2) (2015) 166–169.
[53] M.I. Love, W. Huber, S. Anders, Moderated estimation of fold change and dispersion for RNA-seq data with DESeq2, Genome Biol. 15 (12) (2014) 550.
[54] C.W. Law, et al., voom: precision weights unlock linear model analysis tools for RNA-seq read counts, Genome Biol. 15 (2) (2014) R29.
[55] A. Subramanian, et al., Gene set enrichment analysis: A knowledge-based approach for interpreting genome-wide expression profiles, Proc. Natl. Acad. Sci. USA 102 (43) (2005) 15545–15550.
[56] S. Hänzelmann, R. Castelo, J. Guinney, GSVA: gene set variation analysis for microarray and RNA-Seq data, BMC Bioinforma. 14 (1) (2013) 7.
[57] T. Wu, et al., clusterProfiler 4.0: A universal enrichment tool for interpreting omics data, Innovation 2 (3) (2021) 100141.
[58] A. Liberzon, et al., The Molecular Signatures Database Hallmark Gene Set Collection, Cell Syst. 1 (6) (2015) 417–425.
[59] N.T. Doncheva, et al., Cytoscape StringApp: Network Analysis and Visualization of Proteomics Data, J. Proteome Res 18 (2) (2019) 623–632.
[60] G. Yu, et al., clusterProfiler: an R Package for Comparing Biological Themes Among Gene Clusters, OMICS A J. Integr. Biol. 16 (5) (2012) 284–287.
[61] M. Dei Cas, et al., An Innovative Lipidomic Workflow to Investigate the Lipid Profile in a Cystic Fibrosis Cell Line, Cells 9 (5) (2020) 1197.
[62] C. Morano, et al., Tip-tip filtration ameliorates single-phase extraction methods for plasma large-scale lipidomics analysis, J. Chromatogr. B 1189 (2022) 123099.
[63] M. Dei Cas, et al., Cholangiocarcinoma cells direct fatty acids to support membrane synthesis and modulate macrophage phenotype, Hepatol. Commun. 9 (6) (2025), https://doi.org/10.1097/HC9.0000000000000717.
[64] S. Kulshrestha, et al., Melatonin partially restores hepatic nocturnin oscillations in experimental models of MASLD, Chronobiol. Int. (2025) 1–14.
[65] Y.-W. Chen, et al., Multitissue single-cell analysis reveals differential cellular and molecular sensitivity between fructose and high-fat high-sucrose diets, Cell Rep. 44 (5) (2025) 115690.
[66] M. Colognesi, D. Gabbia, S. De Martin, Depression and Cognitive Impairment-Extrahepatic Manifestations of NAFLD and NASH, Biomedicines 8 (7) (2020), https://doi.org/10.3390/biomedicines8070229.
[67] M. Blüher, An overview of obesity-related complications: The epidemiological evidence linking body weight and other markers of obesity to adverse health outcomes, Diabetes Obes. Metab. 27 (S2) (2025) 3–19.

[68] L. Pitois, et al., Affective responses in adults with severe obesity living or not with a mental disorder during two consecutive 6-min walking exercises, L'Encéphale (2025) S0013700625000326.
[69] G. Gao, et al., Control of lipid droplet fusion and growth by CIDE family proteins, Biochimica et Biophysica Acta (BBA) Molecular Cell Biology Lipids 1862 (10) (2017) 1197–1204.
[70] W. Xu, et al., Differential Roles of Cell Death-inducing DNA Fragmentation Factor-α-like Effector (CIDE) Proteins in Promoting Lipid Droplet Fusion and Growth in Subpopulations of Hepatocytes, J. Biol. Chem. 291 (9) (2016) 4282–4293.
[71] C.E. Geisler, B.J. Renquist, Hepatic lipid accumulation: cause and consequence of dysregulated glucoregulatory hormones, J. Endocrinol. 234 (1) (2017) R1–R21.
[72] D.H. Ipsen, J. Lykkesfeldt, P. Tveden-Nyborg, Molecular mechanisms of hepatic lipid accumulation in non-alcoholic fatty liver disease, Cell Mol. Life Sci. 75 (18) (2018) 3313–3327.
[73] S.A. Willis, et al., The role of hepatic lipid composition in obesity-related metabolic disease, Liver Int. 41 (12) (2021) 2819–2835.
[74] C.F. Chin, et al., Blood-derived lysophospholipid sustains hepatic phospholipids and fat storage necessary for hepatoprotection in overnutrition, J. Clin. Investig. 133 (17) (2023) e171267.
[75] J.J. Lee, et al., Palmitoleic acid is elevated in fatty liver disease and reflects hepatic lipogenesis, Am. J. Clin. Nutr. 101 (1) (2015) 34–43.
[76] M.C. Petersen, G.I. Shulman, Roles of Diacylglycerols and Ceramides in Hepatic Insulin Resistance, Trends Pharmacol. Sci. 38 (7) (2017) 649–665.
[77] A. Gomez-Larrauri, et al., The critical roles of bioactive sphingolipids in inflammation, J. Biol. Chem. 301 (8) (2025) 110475.
[78] J. Han, Y. Wang, mTORC1 signaling in hepatic lipid metabolism, Protein Cell 9 (2) (2018) 145–151.
[79] M. Karin, J.Y. Kim, MASH as an emerging cause of hepatocellular carcinoma: current knowledge and future perspectives, Mol. Oncol. 19 (2) (2025) 275–294.
[80] M. Zhang, et al., Structural insights into tryptamine psychedelics: The role of hydroxyl indole ring site in 5-HT2A receptor activation and psychedelic-like activity, Eur. J. Med. Chem. 281 (2025) 117049.
[81] W.G. Choi, et al., Inhibiting serotonin signaling through HTR2B in visceral adipose tissue improves obesity-related insulin resistance, J. Clin. Investig. 131 (23) (2021) e145331.
[82] Y. Nozaki, et al., Metabolic control analysis of hepatic glycogen synthesis in vivo, Proc. Natl. Acad. Sci. USA 117 (14) (2020) 8166–8176.
[83] D.S. Allende, et al., Glycogenosis is common in nonalcoholic fatty liver disease and is independently associated with ballooning, but lower steatosis and lower fibrosis, Liver Int. 41 (5) (2021) 996–1011.
[84] H.-S. Han, et al., Regulation of glucose metabolism from a liver-centric perspective, Exp. Mol. Med 48 (2016) e218.
[85] D. Santoleri, P.M. Titchenell, Resolving the Paradox of Hepatic Insulin Resistance, Cell. Mol. Gastroenterol. Hepatol. 7 (2) (2019) 447–456.
[86] M.J. Saad, et al., Modulation of insulin receptor, insulin receptor substrate-1, and phosphatidylinositol 3-kinase in liver and muscle of dexamethasone-treated rats, J. Clin. Invest 92 (4) (1993) 2065–2072.
[87] M.J. Saad, et al., Regulation of insulin receptor substrate-1 in liver and muscle of animal models of insulin resistance, J. Clin. Invest 90 (5) (1992) 1839–1849.
[88] J.P. Nogueira, K. Cusi, Role of Insulin Resistance in the Development of Nonalcoholic Fatty Liver Disease in People With Type 2 Diabetes: From Bench to Patient Care, Diabetes Spectr. 37 (1) (2024) 20–28.
[89] F. Bifari, et al., Multiple target tissue effects of GLP-1 analogues on non-alcoholic fatty liver disease (NAFLD) and non-alcoholic steatohepatitis (NASH), Pharmacol. Res. 137 (2018) 219–229.
[90] L.J. Aronne, et al., Tirzepatide as Compared with Semaglutide for the Treatment of Obesity, N. Engl. J. Med (2025) NEJMoa2416394.
[91] I.R. Tough, et al., Paracrine relationship between incretin hormones and endogenous 5-hydroxytryptamine in the small and large intestine, Neurogastroenterol. Motil. 35 (8) (2023) e14589.
[92] E. Badoer, Cardiovascular and Metabolic Crosstalk in the Brain: Leptin and Resistin, Front Physiol. 12 (2021) 639417.
[93] V. Boccardi, Sarcopenia: A dive into metabolism to promote a multimodal, preventive, and regenerative approach, Mech. Ageing Dev. 219 (2024) 111941.
[94] A. Guo, et al., FGF19 protects skeletal muscle against obesity-induced muscle atrophy, metabolic derangement and abnormal irisin levels via the AMPK/SIRT-1/PGC-α pathway, J. Cell. Mol. Med. 25 (7) (2021) 3585–3600.
[95] E. Randrianarisoa, et al., AMPK Subunits Harbor Largely Nonoverlapping Genetic Determinants for Body Fat Mass, Glucose Metabolism, and Cholesterol Metabolism, J. Clin. Endocrinol. Metab. 105 (1) (2020) 14–25.
[96] W. Lu, et al., Role of adipokines in sarcopenia, Chin. Med. J. 136 (15) (2023) 1794–1804.
[97] N. Liu, et al., Requirement of MEF2A, C, and D for skeletal muscle regeneration, Proc. Natl. Acad. Sci. USA 111 (11) (2014) 4109–4114.
[98] G. Navarro, et al., The role of androgens in metabolism, obesity, and diabetes in males and females, Obes. (Silver Spring) 23 (4) (2015) 713–719.
[99] J. Kim, et al., Inhibition of androgen receptor can decrease fat metabolism by decreasing carnitine palmitoyltransferase I levels in skeletal muscles of trained mice, Nutr. Metab. (Lond.) 16 (1) (2019) 82.
[100] K. Ghaibour, et al., Androgen receptor coordinates muscle metabolic and contractile functions, J. Cachex.. Sarcopenia Muscle 14 (4) (2023) 1707–1720.
[101] A.M. Isidori, et al., Leptin and Androgens in Male Obesity: Evidence for Leptin Contribution to Reduced Androgen Levels*, J. Clin. Endocrinol. Metab. 84 (10) (1999) 3673–3680.
[102] A. Yoshiko, et al., Serum Adiponectin and Leptin Is Not Related to Skeletal Muscle Morphology and Function in Young Women, J. Endocr. Soc. 7 (5) (2023) bvad032.
[103] J. Lee, et al., Withaferin A is a leptin sensitizer with strong antidiabetic properties in mice, Nat. Med 22 (9) (2016) 1023–1032.
[104] V.K. Yadav, et al., A Serotonin-Dependent Mechanism Explains the Leptin Regulation of Bone Mass, Appetite, and Energy Expenditure, Cell 138 (5) (2009) 976–989.
[105] S. Park, et al., Inhibition of serotonin-Htr2b signaling in skeletal muscle mitigates obesity-induced insulin resistance, Exp. Mol. Med 57 (6) (2025) 1177–1188.
[106] B. Wang, F.F. Chehab, Deletion of the serotonin 2c receptor from transgenic mice overexpressing leptin does not affect their lipodystrophy but exacerbates their diet-induced obesity, Biochem. Biophys. Res. Commun. 351 (2) (2006) 418–423.